nature neuroscience

TECHNICAL REPORT

https://doi.org/10.1038/s41593-019-0568-z

Cell-type-specific drug-inducible protein synthesis inhibition demonstrates that memory consolidation requires rapid neuronal translation

Prerana Shrestha[1,3], Pinar Ayata[2,3], Pedro Herrero-Vidal[1], Francesco Longo[1], Alexandra Gastone[1], Joseph E. LeDoux[1], Nathaniel Heintz[2*] and Eric Klann[1*]

New protein synthesis is known to be required for the consolidation of memories, yet existing methods of blocking translation lack spatiotemporal precision and cell-type specificity, preventing investigation of cell-specific contributions of protein synthesis. Here we developed a combined knock-in mouse and chemogenetic approach for cell-type-specific drug-inducible protein synthesis inhibition that enables rapid and reversible phosphorylation of eukaryotic initiation factor 2α, leading to inhibition of general translation by 50% in vivo. We use cell-type-specific drug-inducible protein synthesis inhibition to show that targeted protein synthesis inhibition pan-neuronally and in excitatory neurons in the lateral amygdala (LA) impaired long-term memory. This could be recovered with artificial chemogenetic activation of LA neurons, although at the cost of stimulus generalization. Conversely, genetically reducing phosphorylation of eukaryotic initiation factor 2α in excitatory neurons in the LA enhanced memory strength but reduced memory fidelity and behavioral flexibility. Our findings provide evidence for a cell-specific translation program during consolidation of threat memories.

Aversive events often lead to long-term associative memories between the environment in which those events were experienced and the threat, such that a salient cue from the event when presented again can elicit species-specific defensive behaviors. Long-term aversive memories are thought to recruit a distributed network of neurons across the brain, including subnuclei within amygdala, hippocampus, and thalamus, as well as neocortex, depending on the brain state, cue complexity and sensory pathways engaged[1,2]. The LA is the central sensory gateway for the amygdaloid complex and is crucially engaged in both the processing and the storage of the associative aversive memories[3,4].

Decades of studies have reported that consolidation of long-term memories (LTMs) requires one or more waves of new protein synthesis after the memory is first encoded[5–8]; however, the use of pharmacological protein synthesis inhibitors (PSIs) in these studies is burdened with limitations. For instance, an extensively used PSI, anisomycin, causes unwanted side effects that include super-induction of immediate early genes, activation of stress signaling pathways, and catecholamine release[9,10]. Pharmacological PSIs also do not discriminate between molecularly heterogeneous cell populations, and thus do not allow manipulation of cell-autonomous protein synthesis. Genetic approaches to alter the translation machinery at the initiation step provide less ambiguous evidence for the role of protein synthesis in memory processes[11,12]. However, constitutive deletion of genes encoding translational control molecules lacks the temporal control needed to convincingly interrogate the role of protein synthesis in memory consolidation. Past attempts at making chemogenetic tools for blocking protein synthesis in vivo have not been successful[13]. Recently, a genetically encoded PSI, based on tet-regulated expression of an atypical class I ribosome inactivating protein, has been used to block translation elongation in vitro, but this system is not yet amenable for in vivo application or for cell-type-specific inhibition of protein synthesis[14].

A key regulatory step in mammalian protein synthesis is the assembly of active eukaryotic initiation factor 2–guanosine triphosphate (eIF2·GTP) and initiator methionyl transfer RNA into a ternary complex that binds the 40S ribosome. Various types of cellular stress engage pathway-specific protein kinases that phosphorylate the α subunit of eIF2 on serine 51 (S51), which converts eIF2 from a substrate to a competitive inhibitor of eIF2B, a guanine exchange factor that promotes the conversion of inactive eIF2·GDP (guanosine diphosphate) to active eIF2·GTP. Thus, phosphorylation of eIF2α stops the recycling of the ternary complex and inhibits general translation[15]. However, phosphorylation of eIF2α also leads to a paradoxical increase in gene-specific translation of transcripts harboring upstream open reading frames (uORFs) by overcoming the inhibitory effects of uORFs on reinitiation at the putative start codon as ternary complexes decline[16]. Dephosphorylation of eIF2α S51 occurs during late-phase long-term potentiation (L-LTP), as well as during consolidation and reconsolidation of associative memories, and is thought to remove the constraint on general translation[12,17].

Here, we have developed a cell-type-specific drug-inducible protein synthesis inhibition (ciPSI) that uses an inducible form of the kinase domain of double-stranded RNA-activated protein kinase (iPKR) as an actuator for phosphorylating endogenous eIF2α on S51. This resulted in 50% reduction in de novo translation followed by rapid clearance of iPKR and phosphorylated (p)-eIF2α S51 within hours after induction in awake behaving mice. We investigated the time-limited role of protein synthesis in pan-neuronal Nes.iPKR mice (with iPKR expression driven by the *Nes* (nestin) promoter) and subsequently in Ca^{2+}–calmodulin-dependent protein kinase 2α (*CamK2a*)-expressing glutamatergic neurons in the

[1]Center for Neural Science, New York University, New York, NY, USA. [2]HHMI Laboratory of Molecular Biology, The Rockefeller University, New York, NY, USA. [3]These authors contributed equally: Prerana Shrestha, Pinar Ayata. *e-mail: heintz@rockefeller.edu; eklann@cns.nyu.edu

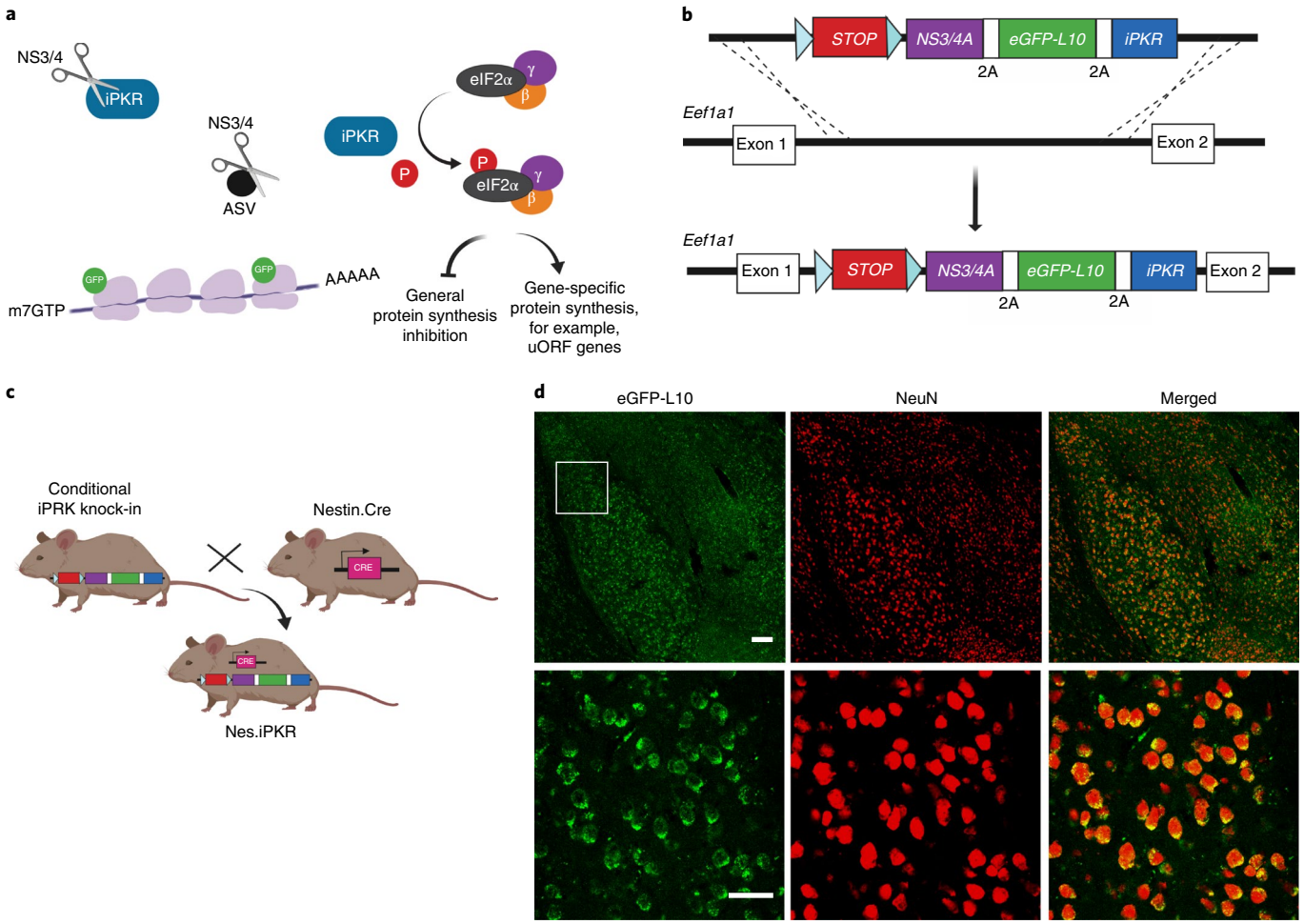

Fig. 1 | Generation of a chemogenetic resource for cell-type-specific protein synthesis inhibition. a, Diagram of the mechanism of action of ciPSI. NS3/4 protease degrades the iPKR kinase domain by binding at the engineered NS5A–5B binding site. NS3/4 inhibitor drug ASV blocks the activity of NS3/4 protease, thereby releasing the PSI iPKR that phosphorylates eIF2α at S51, resulting in an inhibition of general translation while permitting gene-specific translation of transcripts harboring a uORF. **b**, Schematic of the knock-in transgenesis approach for the ciPSI iPKR cassette into the *Eef1a1* genomic locus. **c**, Pan-neuronal Nes.iPKR mice were generated by breeding Nes.Cre and iPKR knock-in mice. **d**, GFP-tagged ribosomal protein L10 is present in the soma of all neurons in the amygdala and completely overlaps with NeuN expression. Representative immunofluorescence image shows expression of GFP-L10a (green) in NeuN$^+$ (red) neurons. The experiment was repeated twice independently with similar results. Inset in the first row is magnified in the second row. Scale bars, 100 µm (top); 50 µm (bottom).

LA during consolidation of auditory threat memory. Such cued threat conditioning (cTC) is particularly amenable to studying the memory consolidation process because one-trial training is sufficient to form a persistent LTM, and a unimodal cue can be used for memory retrieval. We found that long-term threat memories are particularly labile to pan-neuronal and LA CamK2α$^+$ cell-type-specific protein synthesis disruption in the first hour after training. We further found that the translation program regulated by phosphorylation status of eIF2α plays an important role in calibrating memory strength and fidelity. Our findings provide mechanistic insight into the nature of long-term threat memory consolidation.

Results

A chemogenetic resource for cell-type-specific protein synthesis inhibition. To induce phosphorylation of eIF2α, we engineered the kinase domain of the eIF2α kinase PKR, to harbor a recognition site (NS5A/B) for a recombinant nonstructural protein 3/4 (NS3/4) protease, which can be chemically inhibited with asunaprevir (ASV)[18,19] (Fig. 1a). We first tested toxicity of ASV in amygdala slices from wild-type (WT) mice infused with an increasing dose of ASV (0, 10 and 100 nM and 1 µM) and determined that for all doses tested, there was no significant induction of either the immediate early gene c-*Fos* or the integrated stress response as assessed by examination of the level of p-eIF2α S51 (Extended Data Fig. 1a). The kinase domain of PKR is a caspase-generated fragment that is constitutively active and does not require either double-stranded RNA or dimerization for activation[20]. We designed our ciPSI multicistronic construct with NS3/4 protease[21], enhanced green fluorescent protein (eGFP) and inducible PKR (iPKR) transgenes separated by self-cleaving 2A proteinase that allows translation of individual elements by ribosome skipping[22] (Extended Data Fig. 1b). To test the inhibition of global translation in vitro, we metabolically labeled newly synthesized proteins with S^{35} methionine after starvation. In cells transfected with iPKR and NS3/4A, iPKR was degraded by NS3/4, and de novo translation was equivalent to the control cells, whereas cells transfected with iPKR plasmid alone in the absence of NS3/4A had substantially reduced translation by about 60%. Unmodified PKR kinase domain (PKRk) similarly reduced de novo translation relative to controls, but the PKRk levels were nonresponsive to NS3/4 protease (Extended Data Fig. 1c). As predicted, PKRk fragment was detected only in lysates from cells transfected with either unmodified PKRk or modified iPKR (Extended Data Fig. 1d).

We next knocked in the ciPSI multicistronic cassette into the first intron of the mouse *Eef1a1* genomic locus[23] with two modifications (Fig. 1b, Supplementary Data 1 and Extended Data Fig. 2a,b). First, eGFP was substituted with an eGFP-L10 fusion to use as a fluorescent marker of cells expressing ciPSI and to eventually enable translating ribosome affinity purification profiling[24]. Second, a STOP cassette flanked by *loxP* sites preceded the ciPSI cassette to allow cell-type-specific disruption of protein synthesis when combined with Cre-driver mouse lines and/or Cre-expressing viruses. These modifications had no effect on expression of iPKR (data not shown). A mouse Nestin (*Nes*) Cre-driver line[25] was bred with the ciPSI line to generate transheterozygote Nes.iPKR pan-neuronal ciPSI knock-in mice, which were viable and fertile. The Nes-iPKR mice expressed eGFP-L10 in all neurons in the amygdala, as marked by complete overlap with neuronal nuclei (NeuN) staining (Fig. 1d), as well as in cortical areas, such as the anterior cingulate cortex and somatosensory cortex, hippocampal areas, CA1 and CA3, and the dentate gyrus (Extended Data Fig. 2c–g). Despite heterozygous deletion of *Eef1a1* allele and expression of the multicistronic cassette in Nes.iPKR mice, the mice displayed normal spontaneous locomotion and thigmotaxis in open field tests (Extended Data Fig. 3a–c).

To test the efficiency of ciPSI in blocking protein synthesis ex vivo, we subjected amygdala slices of Nes.iPKR and WT mice to bio-orthogonal noncanonical amino acid tagging (BONCAT) (ref. [26]) of newly synthesized proteins. Nes.iPKR amygdala slices treated with 1 µM ASV exhibited a sharp decline in de novo translation (~80%) compared with controls (Fig. 2a). Because BONCAT uses azidohomoalanine (AHA), a synthetic methionine analog, which can get outcompeted by endogenous methionine in vivo, this method does not sufficiently label de novo translation in vivo. Thus, an independent method of labeling de novo translation, surface sensing of translation (SUnSET) (ref. [27]), which measures translation elongation and is amenable for in vivo labeling, was used to test ciPSI efficiency in awake behaving mice. SUnSET immunoblotting showed that Nes.iPKR mice centrally infused with 150 pg ASV exhibited a robust decrease in protein synthesis (~50%) compared with controls (Fig. 2b). The inhibition of protein synthesis was concomitant with a specific increase in phosphorylation of eIF2α at 1 h after ASV treatment both ex vivo (Fig. 2c) and in vivo (Fig. 2d), with no effect on either the extracellular signal-regulated kinases 1/2 (ERK1/2) or mechanistic target of rapamycin (mTORC1) pathways (Fig. 2d). Next, we investigated the ASV pharmacokinetics in Nes.iPKR amygdala lysates by harvesting tissue at increasing time points after drug infusion. We found that peak expression of iPKR is reached at 0.5 h, which steadily declines at 1 and 3 h, and is completely degraded by 6 h (Fig. 2e). Subsequently, phosphorylation of eIF2α steadily increased at 0.5 and 1 h and then declined to baseline at 3 h. As a result of phosphorylation of eIF2α, proteins whose transcripts harbor uORFs, specifically ATF4 and GADD34, accumulated and remained at higher levels compared with control until 3 h (Fig. 2e). GADD34 is the regulatory subunit of the eIF2α S51 phosphatase[16], and the negative feedback caused by increased GADD34 levels combined with the degradation of iPKR by NS3/4 protease at the 3-h time point might be responsible for reduced phosphorylation of eIF2α below the control (Fig. 2e). We also probed for c-Fos to assess whether c-Fos levels change with ciPSI, and found that c-Fos levels significantly decrease below baseline at 3 and 6 h after ASV treatment (Fig. 2e), indicating general translation suppression.

Past studies have shown that the enduring L-LTP in amygdala requires protein synthesis[28,29]. To determine whether chemogenetic inhibition of pan-neuronal protein synthesis influences synaptic plasticity, we examined LTP of LA. We delivered three trains of high-frequency stimulation (HFS) to thalamo–amygdalar inputs and recorded the field excitatory postsynaptic potential (fEPSP) in the dorsal subdivision of LA while perfusing into the amygdala slices 5 nM ASV 10 min before and for 90 min after tetanus.

Fig. 2 | Drug-induced neuronal protein synthesis inhibition. a, De novo translation labeled at the amino terminus (N terminus) using BONCAT in Nes.iPKR amygdala slices showed a robust decrease in translation in mutant amygdala treated with 1 µM ASV compared with VEH-treated mutant amygdala (****$P < 0.0001$), as well as ASV-treated WT amygdala (****$P < 0.0001$). $n = 3$ independent lysates from three mice per group. Two-way ANOVA with Bonferroni's post hoc test was conducted. Genotype–drug interaction: $F(1,8) = 34.6$, $P = 0.0004$; drug: $F(1,8) = 75.2$, $P < 0.0001$; genotype: $F(1,8) = 80.7$, $P < 0.0001$. **b**, De novo translation labeled at the carboxy terminus (C terminus) in awake behaving mice using SUnSET also showed a significant decrease in translation in mutant mice infused with 150 pg ASV (100 nM in 2 µl) compared with VEH infusion (***$P < 0.001$), as well as in WT mice infused with ASV (****$P < 0.0001$). $n = 3$ independent lysates from two mice per group. Two-way ANOVA with Bonferroni's post hoc test was conducted. Genotype–drug interaction: $F(1,8) = 19.49$, $P = 0.0022$; drug: $F(1,8) = 41.51$, $P = 0.0002$; genotype: $F(1,8) = 117.9$; $P < 0.0001$. **c**, Bath application of 1 µM ASV caused a robust phosphorylation of eIF2α in mutant Nes.iPKR amygdala slices compared with ASV-treated WT slices and VEH-treated Nes.iPKR slices (****$P < 0.0001$). $n = 3$ independent lysates from three mice per group. Two-way ANOVA with Bonferroni's post hoc test was conducted. Genotype–drug interaction: $F(1,8) = 44.7$, $P = 0.0002$; drug: $F(1,8) = 53.5$, $P < 0.0001$; genotype: $F(1,8) = 51.7$, $P < 0.0001$. **d**, ASV infusion in vivo (150 pg or 100 nM in 2 µl) also caused a significant increase in p-eIF2α in Nes.iPKR amygdala compared with controls (****$P < 0.0001$). $n = 3$ independent lysates from three mice per group. Two-way ANOVA with Bonferroni's post hoc test was conducted. Genotype–drug interaction: $F(1,8) = 70.87$, $P < 0.0001$; drug: $F(1,8) = 19.04$, $P < 0.0024$; genotype: $F(1,8) = 120.4$, $P < 0.0001$. Major intracellular signaling pathways, ERK1/2, mitogen-activated protein kinase and mTORC1, assessed by examining p-ERK1/2 (T202/Y204) and p-S6 (S240/244) levels, were unchanged by ASV treatment in *Nes.iPKR* amygdala lysates. n(p/t-eIF2α) = 3 independent lysates from three mice per group; n(p/t-ERK1/2 in WT+VEH and WT+ASV) = 4 independent lysates per group; n(Nes.iPKR+VEH and Nes.iPKR+ASV) = 3 independent lysates from three mice per group, n(p/t-S6) = 3 independent lysates per group. Two-way ANOVA followed by post hoc Bonferroni's test was conducted. **e**, Time course for ciPSI carried out by collecting amygdala lysate at different time points after ASV infusion (0, 0.5, 1, 3 and 6 h) shows peak expression of 36 kDa iPKR at 0.5 h, which was undetectable at 6 h (****$P < 0.0001$). Endogenous PKR (68 kDa) remained unchanged after ASV treatment. Peak expression of p-eIF2α, normalized for t-eIF2α, was achieved at 0.5 h after ASV infusion followed by a steady decline from 3 h onward (*$P < 0.05$). ATF4 and GADD34 proteins whose transcripts harbor a uORF were increased by ASV by 1 h and declined to baseline by 6 h (***$P < 0.001$, **$P < 0.01$). c-FOS levels significantly declined from baseline at 3 and 6 h postinfusion (**$P < 0.01$, ***$P < 0.001$). $n = 3$ independent lysates per group; repeated-measures one-way ANOVA with post hoc Bonferroni's test. **f**, Schematic for L-LTP recording in the LA (top) and representative field potentials before (1) and 90 min after tetanus (2) for different groups of slices are shown (bottom). L-LTP evoked by three trains of HFS was impaired in Nes.iPKR amygdala slices treated with ASV (5 nM) applied before the tetanus and perfused for 90 min after tetanus (****$P < 0.0001$; n(WT + VEH) = 12 slices, n(WT + ASV) = 12 slices, n(Nes.iPKR + VEH) = 13 slices and n(Nes.iPKR + ASV) = 15 slices). One-way ANOVA with Bonferroni's post hoc test was performed. **g**, Mean fEPSPs at baseline (10 min) before ASV application, at 30 min (that is, 10 min after ASV application), at 60 min (30 min after tetanus) and at 120 min (90 min after tetanus). ASV significantly reduced fEPSP slope in Nes.iPKR amygdala at 120 min compared with VEH treatment (***$P < 0.01$) and ASV-treated WT amygdala (****$P < 0.001$), but had no effect on baseline (n(WT + VEH) = 12 slices, n(WT + ASV) = 12 slices, n(Nes.iPKR + VEH) = 13 slices and n(Nes.iPKR + ASV) = 15 slices). Two-way ANOVA with Bonferroni's post hoc test. Genotype–drug–time interaction: $F(6,144) = 4.700$, $P = 0.0002$; genotype–drug: $F(2,144) = 172.5$, $P < 0.0001$; time: $F(3,144) = 5.999$, $P = 0.0007$. Data are presented as mean ± s.e.m.

We found that L-LTP was significantly inhibited by ASV-induced release of iPKR (Fig. 2f). The drug had no effect on baseline fEPSP slope in both WT and Nes.iPKR slices (Fig. 2g). The inhibition had a rapid onset after tetanus and became more robust during L-LTP maintenance (Fig. 2g). Together, these results indicate that chemogenetic inhibition of protein synthesis impairs both induction and expression of L-LTP.

Temporally structured protein synthesis is required for LTM consolidation. Given our approach that bypasses the limitations and side effects of methods used to study protein synthesis in vivo, we could now study the role of de novo protein synthesis in memory consolidation. We trained Nes.iPKR and control mice in simple auditory threat conditioning and centrally infused ASV immediately after training (Fig. 3a). Nes.iPKR and WT mice were

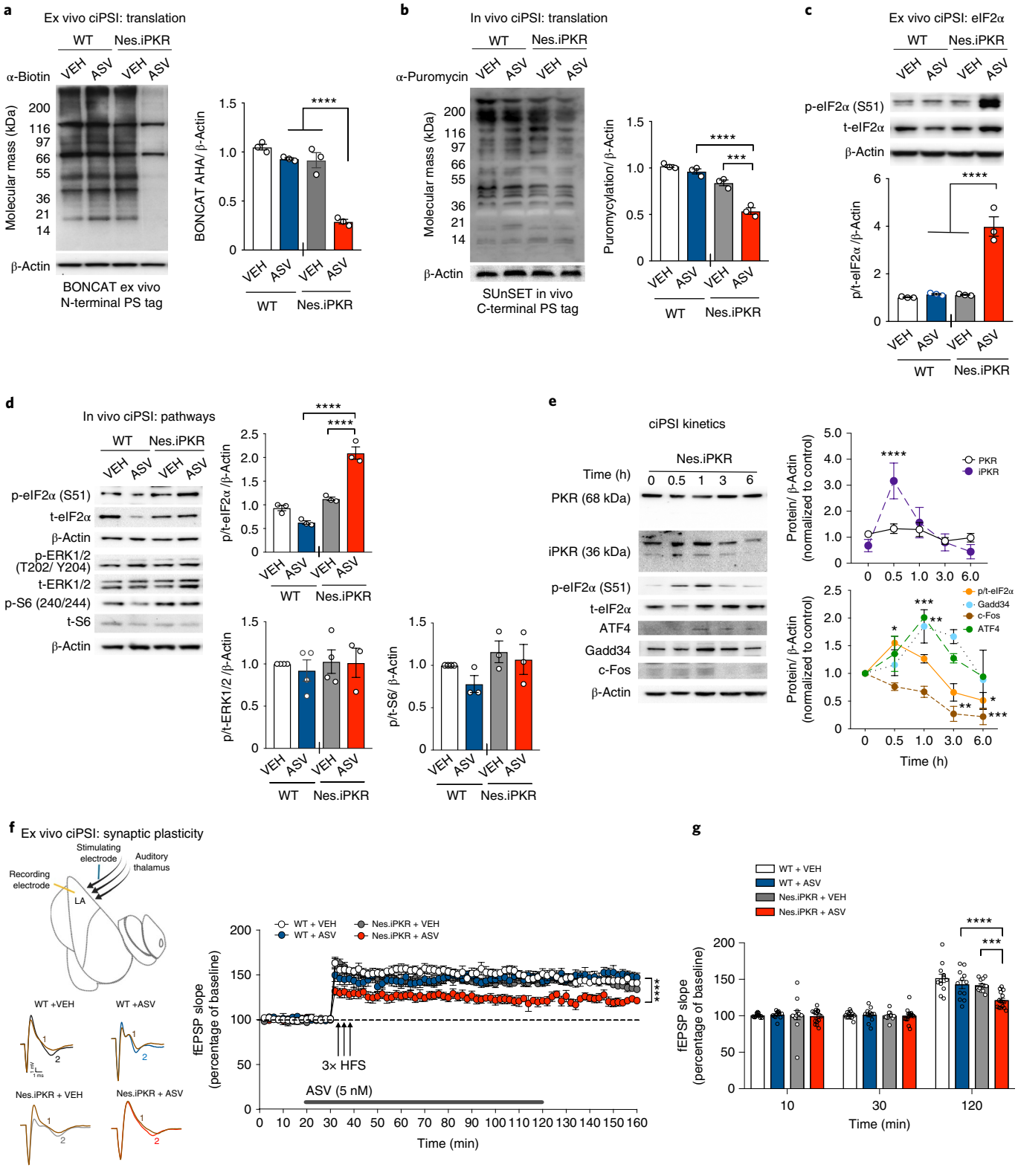

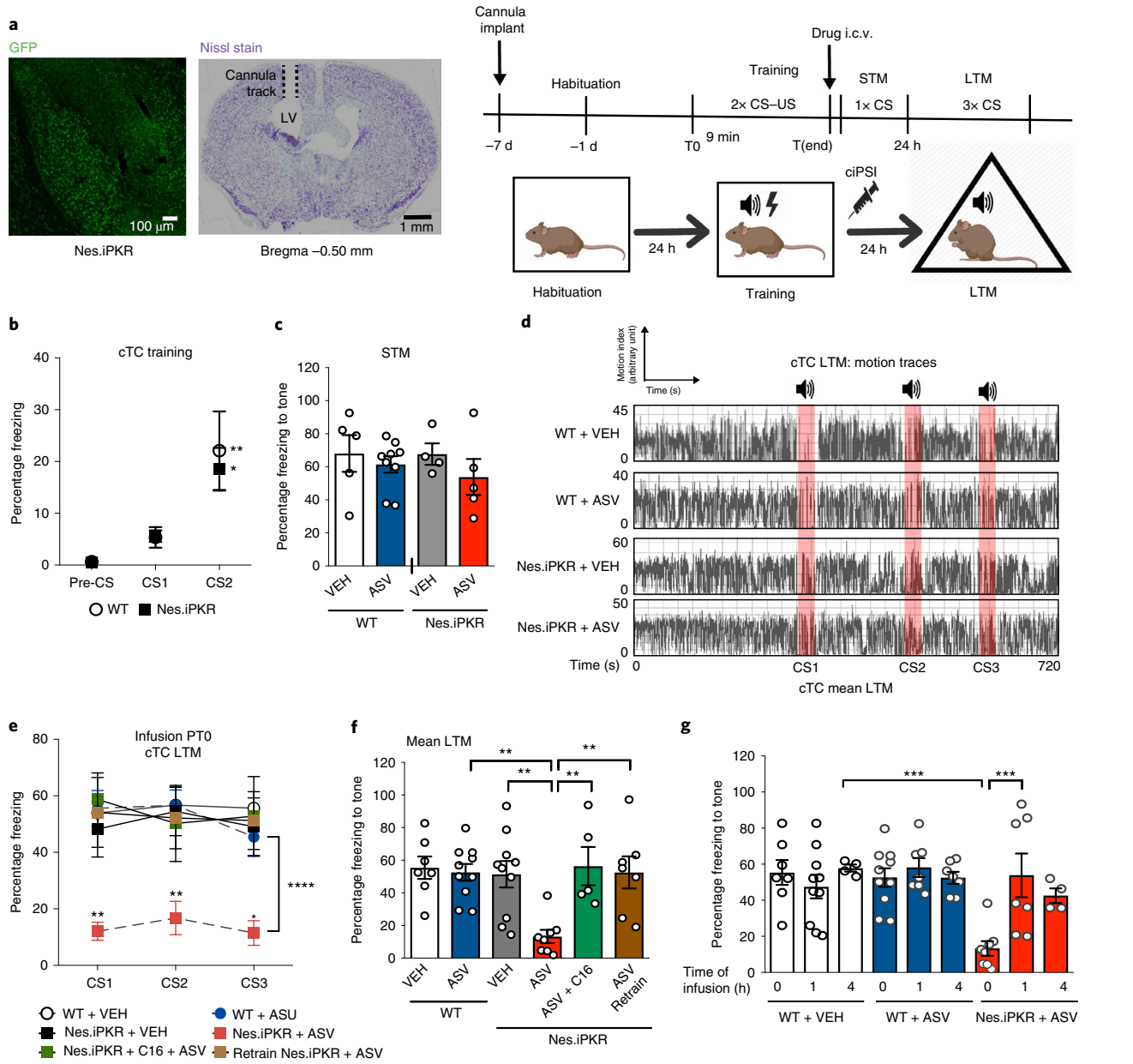

Fig. 3 | Temporally structured protein synthesis is required for LTM consolidation. a, Locations of cannula implants for all experimental animals subjected to i.c.v. infusion were verified with post hoc histology. Schematic of the experimental paradigm (right) for simple cTC in Nes.iPKR mice pan-neuronally expressing the ciPSI system. **b**, Nes.iPKR animals learn the association between CS and US (CS2 versus CS1: $^{*}P < 0.05$) similar to the WT mice ($^{**}P < 0.01$; n(WT) = 13 animals and n(Nes.iPKR) = 16 animals). Repeated-measures two-way ANOVA with Bonferroni's post hoc test was performed. CS: $F(2,54) = 19.38$; $P < 0.0001$. **c**, Nes.iPKR mice infused with ASV were comparable in STM performance as VEH-infused mice and WT controls. n(WT+VEH) = 5 animals, n(WT+ASV) = 9 animals, n(Nes.iPKR+VEH) = 4 animals and n(Nes.iPKR+ASV) = 5 animals. Ordinary one-way ANOVA was conducted. $F(3,19) = 0.576$, $P = 0.638$ (not significant). **d**, Representative motion traces for WT mice infused with VEH or ASV and for Nes. iPKR mice infused with VEH or ASV. **e**, LTM tested 24 h after training was significantly impaired for Nes.iPKR mice infused with ASV compared with controls for all three CS presentations. Pretraining administration of the PKR inhibitor C16 rescued the memory deficit in Nes.iPKR mice infused with ASV for all three CS presentations. Retraining the Nes.iPKR mice that previously underwent ciPSI-mediated amnesia fully recovered LTM for all three CS presentations ($P < 0.05$; n(WT+VEH) = 7 animals, n(WT+ASV) = 10 animals, n(Nes.iPKR+ASV) = 8 animals, n(Nes.iPKR+ASV+C16) = 5 animals and n(Nes.iPKR+ASV/retrain) = 7 animals). Repeated-measures two-way ANOVA with Bonferroni's post hoc test was performed. Genotype: $F(5,40) = 4.570$, $P = 0.0022$. **f**, cTC mean LTM was significantly impaired for Nes.iPKR animals treated with ASV compared with VEH ($^{*}P = 0.021$) and WT mice infused with ASV ($^{**}P = 0.0015$). cTC mean LTM in Nes.iPKR mice was rescued with C16, compared with Nes.iPKR mice infused with ASV alone ($^{**}P = 0.0041$). cTC mean LTM2 in retrained Nes.iPKR mice was comparable with WT mice. n(WT+VEH) = 7 animals, n(WT+ASV) = 10 animals, n(Nes.iPKR+ASV) = 8 animals, n(Nes.iPKR+ASV+C16) = 5 animals and n(Nes.iPKR+ASV/retrain) = 7 animals. One-way ANOVA with Bonferroni's post hoc test was performed. $F(5,41) = 4.890$, $P = 0.0013$. **g**, The LTM deficit was present only for Nes.iPKR mice infused with ASV immediately after training ($^{***}P = 0.0002$), but not 1 h ($^{***}P = 0.0004$) or 4 h after training. One-way ANOVA with Bonferroni's post hoc test was conducted. n(WT+VEH, 0 h) = 7 animals, n(WT+VEH, 1 h) = 10 animals, n(WT+VEH, 4 h) = 4 animals, n(WT+ASV, 0 h) = 10 animals, n(WT+ASV, 1 h) = 7 animals, n(WT+ASV, 4 h) = 7 animals, n(Nes. iPKR+ASV, 0 h) = 8 animals, n(Nes.iPKR+ASV, 1 h) = 7 animals and n(Nes.iPKR+ASV, 4 h) = 4 animals. Data are presented as mean ± s.e.m. LV, lateral ventricle; US, unconditioned stimulus. $^{*}P < 0.05$, $^{**}P < 0.01$, $^{***}P < 0.001$.

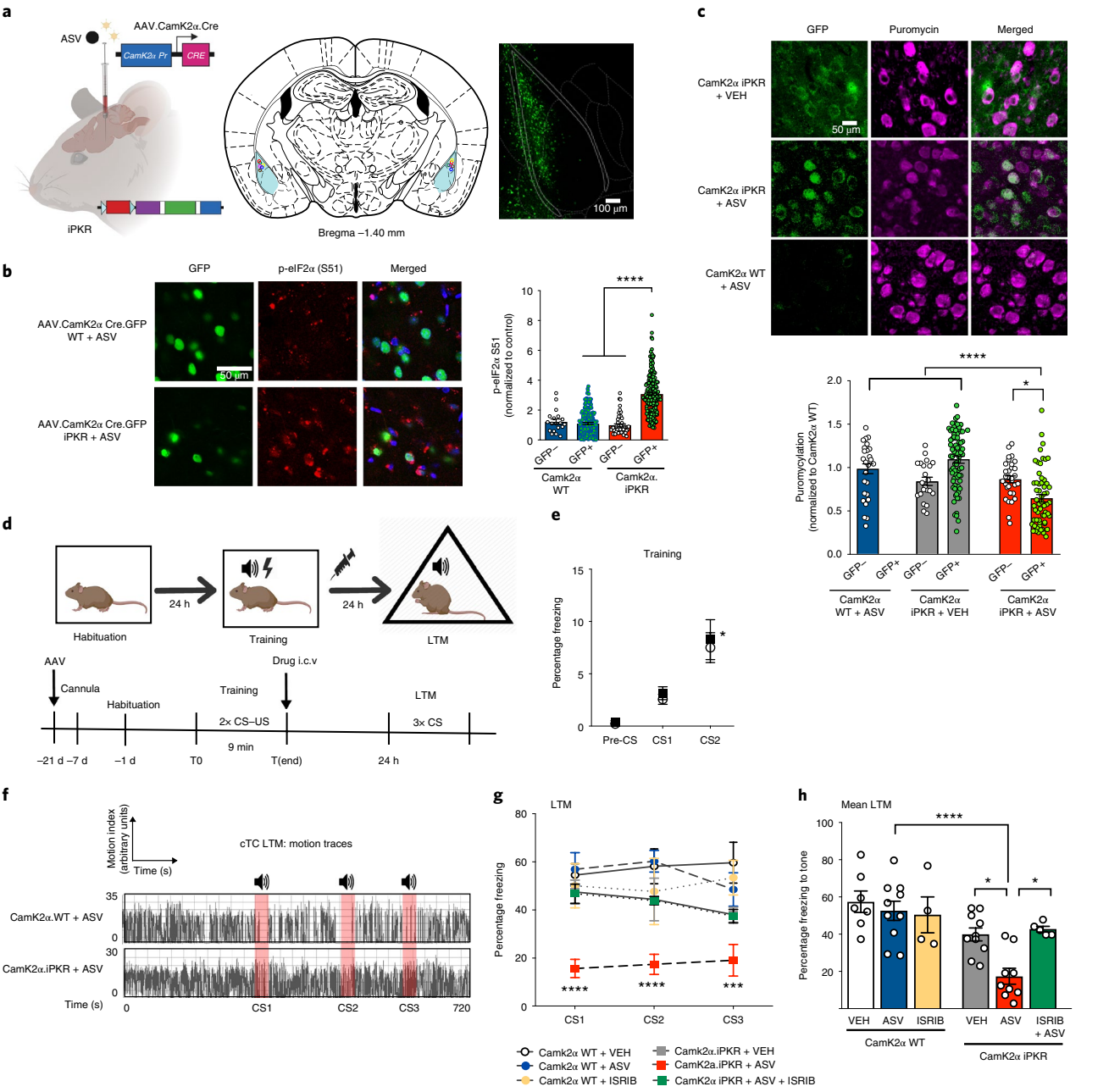

Fig. 4 | Cell-type-specific protein synthesis inhibition in principal neurons in the LA. a, CamK2α.iPKR mice were generated by bilaterally injecting AAV1.CamK2α.Cre (or AAV9.CamK2α.Cre.eGFP) into the LA of iPKR mice. **b**, ASV infusion caused a significant increase in p-eIF2α levels in GFP$^+$ neurons in CamK2α.iPKR mice compared with GFP$^-$ neighboring neurons in the LA (****$P < 0.0001$), as well as GFP$^+$ neurons in CamK2α WT mice (****$P < 0.0001$). Both WT and iPKR mice were injected with AAV.CamK2α.Cre.GFP in the LA. n(CamK2α WT+ASV) = 19 GFP$^-$ neurons and 170 GFP$^+$ neurons; n(CamK2α.iPKR +ASV) = 49 GFP$^-$ neurons and 193 GFP$^+$ neurons from three mice per group. Two-way ANOVA with Bonferroni's post hoc test was conducted. Genotype–GFP interaction: $F(1, 427) = 45.11$, $P < 0.0001$; genotype: $F(1, 427) = 28.53$, $P < 0.0001$; GFP: $F(1, 427) = 36.75$, $P < 0.00001$. **c**, In vivo SUnSET assay: ASV-treated CamK2α.iPKR mice have significantly reduced translation in LA principal neurons compared with VEH treatment (****$P < 0.0001$) and ASV-treated WT mice (****$P < 0.0001$). One-way ANOVA followed by Bonferroni's post hoc test was performed. n(CamK2α WT+ASV) = 36 GFP$^-$ neurons, n(CamK2α.iPKR+VEH) = 22 GFP$^-$ neurons and 78 GFP$^+$ neurons, and n(CamK2α.iPKR+ASV) = 31 GFP$^-$ neurons and 58 GFP$^+$ neurons from three mice per group. **d**, Schematic of experimental paradigm for cTC in CamK2α.iPKR mice. **e**, CamK2α.iPKR mice were comparable with WT in learning the CS–US association (*$P = 0.07$). Repeated-measures two-way ANOVA with Bonferroni's post hoc test. n(CamK2α WT) = 5 animals and n(CamK2α.iPKR) = 5 animals. CS: $F(2,24) = 24.93$, $P < 0.0001$. **f**, Representative cTC LTM motion traces for CamK2α WT and CamK2α.iPKR. **g**, CamK2α.iPKR mice receiving ASV infusion immediately after training displayed a severe LTM deficit across all three CS presentations (****$P < 0.0001$) that was rescued with pretraining infusion of ISRIB. n(CamK2α WT+VEH) = 7 animals, n(CamK2α WT+ASV) = 9 animals, n(CamK2α WT+ISRIB) = 4 animals, n(CamK2α.iPKR+VEH) = 10 animals, n(CamK2α.iPKR+ASV) = 9 animals and n(CamK2α.iPKR+ASV+ISRIB) = 5 animals. Repeated-measures two-way ANOVA with Bonferroni's post hoc test was performed. Genotype: $F(5,35) = 9.767$, $P < 0.0001$. **h**, cTC mean LTM was impaired in CamK2α.iPKR mice infused with ASV (****$P < 0.0001$) but was rescued by ISRIB administration (*$P < 0.05$). One-way ANOVA with Bonferroni's post hoc test. n(CamK2α WT+VEH) = 7 animals, n(CamK2α WT+ASV) = 9 animals, n(CamK2α WT+ISRIB) = 4 animals, n(CamK2α.iPKR+VEH) = 10 animals, n(CamK2α.iPKR+ASV) = 9 animals and n(CamK2α.iPKR+ASV+ISRIB) = 5 animals. Data are presented as mean ± s.e.m.

comparable in learning the association of tone with footshock, as well as in short-term memory (STM) that is protein synthesis independent (Fig. 3b,c). However, when the animals were tested for LTM 24 h later, Nes.iPKR mice infused with ASV exhibited markedly reduced defensive behavior in response to the paired tone presentations, even though outside of tone presentations the mice had similar motion indices (Fig. 3d–f). Our findings are consistent with previous studies that showed deletion of genes encoding eIF2α kinases, *Gcn2* and *Pkr*, led to an enhancement of long-term spatial and threat memories, and decreased the threshold for L-LTP induction[30,31]. To ensure that ciPSI did not permanently damage the memory system, we retrained Nes.iPKR mice previously infused with ASV in the auditory threat conditioning paradigm. Nes.iPKR mice fully recovered LTM and exhibited a species-appropriate defensive response to the conditioned tone (Fig. 3e,f). Because Nes.iPKR mice express viral NS3/4 protease in addition to the actuator iPKR, we tested the molecular specificity of ciPSI with the PKR inhibitor C16, which binds to PKR at the ATP binding site, thereby blocking its kinase activity[32]. Pretraining administration of C16 inhibited the activation of iPKR and prevented the LTM deficit in Nes.iPKR mice (Fig. 3e,f). Depending on the training paradigm, there are multiple critical periods during memory consolidation that are sensitive to protein synthesis inhibition[7,33]. Therefore, we assessed whether consolidation of associative threat memory in our paradigm requires one or more waves of de novo translation by inducing ciPSI at 0, 1 and 4 h after training (Fig. 3g). Only Nes.iPKR mice receiving ASV infusion immediately after training displayed LTM deficit (Fig. 3g), suggesting that there is only one wave of protein synthesis for up to 4 h after training in our paradigm.

Cell-type-specific de novo translation in LA CamK2α-positive neurons is necessary for LTM consolidation. Lesioning and functional inactivation studies have shown that the LA is an integral brain structure for the formation and storage of conditioned aversive memories[3,34,35]. Learned threat elicits persistent cortical and thalamic input-specific synaptic potentiation in principal excitatory neurons within the LA[36,37]. Thus, we asked whether de novo protein synthesis in CamK2α-positive principal neurons in LA is necessary for aversive memory consolidation. We virally delivered CamK2α.Cre.eGFP into the bilateral LA of iPKR mice and control mice (Fig. 4a). Phosphorylation of eIF2α was specifically increased in neurons from CamK2α.iPKR mice (expressing iPKR from the *CamK2a* promoter) compared with WT mice and non-eGFP-positive neurons in the same animals (Fig. 4b) with a corresponding decrease in de novo translation (Fig. 4c) upon ASV administration. CamK2α.iPKR mice were threat conditioned as described previously and centrally infused with ASV immediately after training (Fig. 4d). CamK2α.iPKR mice were comparable with WT controls in memory acquisition (Fig. 4e), but LTM tested 24 h later was significantly impaired (Fig. 4f–h). This LTM consolidation deficit with ciPSI was prevented by pretraining administration of ISRIB (integrated stress response inhibitor), a drug that rescues the p-eIF2α-mediated constraint on general translation by enhancing the activity of eIF2B (Fig. 4g,h)[38]. We also tested ASV-treated CamK2α.iPKR mice in an open field test and elevated plus maze to gauge anxiety-related behaviors, and found that although spontaneous locomotion was normal in these animals, there was a significant increase in the percentage of time spent in the open arm, indicating reduced anxiety-related behavior (Extended Data Fig. 4a–e).

It is evident that the translation program regulated by eIF2α is necessary for LTM consolidation; however, the physiological accumulation of ATF4 as a result of increased eIF2α phosphorylation raises the question of whether it is either decreased protein synthesis or increased ATF4 levels causing the memory deficit. Indeed, a previous study has reported that even in the absence of translation inhibition, the p-eIF2α-mediated increase in ATF4 levels can cause memory deficit by transcriptional repression of CREB-regulated genes[13]. Dissociating the effects of general

Fig. 5 | Bidirectional control of memory strength by phosphorylation of eIF2α S51 in LA principal neurons. a, Heterozygous CamK2α.eIF2α (A/+) and homozygous CamK2α.eIF2α (A/A) were generated by bilaterally injecting AAV1.CamK2α.Cre into the LA of eIF2α (S51A) CAG $Pr^{fl.eIF2\alpha.fl.GFP}$ mice. **b**, In vivo SUnSET assay: homozygous CamK2α.eIF2α (A/A) mice displayed a significant increase in de novo translation compared with the CamK2α WT mice and heterozygous CamK2α.eIF2α (A/+) mice (****$P < 0.0001$). n(CamK2α WT) = 101 neurons from three mice, n(CamK2α eIF2α (A/+)) = 93 neurons from three mice and n(CamK2α.eIF2α (A/A)) = 93 neurons from three mice. One-way ANOVA followed by Bonferroni's post hoc test was performed. $F(2, 284) = 52.01$, $P < 0.0001$. **c**, Double-transgenic iPKR eIF2α (A/+) and iPKR eIF2α (A/A) mice were bilaterally injected with AAV1.CamK2α.Cre in the LA to generate CamK2α.iPKR eIF2α (A/+) and CamK2α.iPKR eIF2α (A/A) mice, respectively. All groups of mice (CamK2α WT, CamK2α eIF2α (A/+), CamK2α.eIF2α (A/A), CamK2α.iPKR eIF2α (A/+) and CamK2α.iPKR eIF2α (A/A)) learned the CS–US association; however, CamK2α.eIF2α (A/A) and CamK2α.iPKR eIF2α (A/A) mice learned better than CamK2α WT mice (CS2: CamK2α WT versus CamK2α.iPKR eIF2α (A/A), ***$P = 0.0009$; CamK2α WT versus CamK2α.eIF2α (A/A), $P = 0.0740$). Repeated-measures two-way ANOVA with Bonferroni's post hoc test was conducted. CS: $F(1,31) = 44.25$, $P < 0.0001$. n(CamK2α WT) = 6 animals, n(CamK2α eIF2α (A/+)) = 4 animals, n(CamK2α eIF2α (A/A)) = 6 animals, n(CamK2α.iPKR eIF2α (A/+)) = 4 animals and n(CamK2α.iPKR eIF2α (A/A)) = 7 animals. **d**, Freeze-frame motion traces for CamK2α WT mice treated with VEH, CamK2α iPKR mice treated with ASV and CamK2α eIF2α (A/A) mice. **e**, In the cTC LTM test, homozygous CamK2α.eIF2α (A/A) mice displayed enhanced memory compared with CamK2α WT mice (**$P < 0.01$), whereas as shown previously, CamK2α.iPKR mice treated with ASV have impaired memory (**$P < 0.01$). Heterozygous CamK2α eIF2α (A/+) mice displayed comparable LTM as WT mice. Heterozygous CamK2α.iPKR eIF2α (A/+) mice treated with ASV exhibited comparable memory deficit as CamK2α iPKR mice treated with ASV. However, the memory deficit in CamK2α.iPKR mice was fully rescued by introducing nonphosphorylatable eIF2α in homozygous CamK2α.iPKR eIF2α (A/A) mice (****$P < 0.0001$). n(CamK2α WT) = 7 animals, n(CamK2α eIF2α (A/+)) = 7 animals, n(CamK2α eIF2α (A/A)) = 10 animals, n(CamK2α.iPKR+ASV) = 7 animals, n(CamK2α.iPKR eIF2α (A/+)+ASV) = 5 animals and n(CamK2α.iPKR eIF2α (A/A)+ASV) = 5 animals. Repeated-measures two-way ANOVA with Bonferroni's post hoc test was performed. Genotype: $F(5,35) = 12.79$, $P < 0.0001$. **f**, Bar graphs for mean cTC LTM for all groups. One-way ANOVA with Bonferroni's post hoc test. $F(5,36) = 23.30$, $P < 0.0001$. n(CamK2α WT) = 6 animals, n(CamK2α eIF2α (A/+)) = 8 animals, n(CamK2α eIF2α (A/A)) = 9 animals, n(CamK2α.iPKR+ASV) = 8 animals, n(CamK2α.iPKR eIF2α (A/+)+ASV) = 5 animals and n(CamK2α.iPKR eIF2α (A/A)+ASV) = 6 animals. **g**, Memory enhancement in CamK2α eIF2α (A/A) mice was accompanied by cognitive inflexibility at the offset of CS. During ITIs, CamK2α eIF2α (A/A) freeze at a much greater rate compared with WT (***$P < 0.001$) and CamK2α eIF2α (A/+) mice (**$P < 0.01$). Similarly, CamK2α.iPKR eIF2α (A/A)+ASV mice displayed a higher freezing rate during the ITIs compared with CamK2α iPKR treated with ASV (*$P < 0.05$). n(CamK2α WT) = 6 animals, n(CamK2α eIF2α (A/+)) = 10 animals, n[CamK2α eIF2α (A/A)) = 10 animals, n(CamK2α.iPKR+ASV) = 5 animals, n(CamK2α.iPKR eIF2α (A/+)+ASV) = 5 animals and n(CamK2α.iPKR eIF2α (A/A)+ASV) = 6 animals. One-way ANOVA with Bonferroni's post hoc test. $F(5,36) = 8.569$, $P < 0.0001$. **h**, During pre-CS, locomotor activity was equivalent across groups. n(CamK2α WT) = 6 animals, n(CamK2α eIF2α (A/+)) = 10 animals, n(CamK2α eIF2α (A/A)) = 10 animals, n(CamK2α.iPKR+ASV) = 5 animals, n(CamK2α.iPKR eIF2α (A/+)+ASV) = 5 animals and n(CamK2α.iPKR eIF2α (A/A)+ASV) = 6 animals. Repeated-measures two-way ANOVA was performed. $F(5,26) = 1.335$, not significant. Data are presented as mean ± s.e.m. *$P < 0.05$, **$P < 0.01$, ***$P < 0.001$, ****$P < 0.0001$.

translation inhibition from that of ATF4 expression on memory processes is not trivial because a pharmacological inhibitor of ATF4 does not exist; moreover, long-term knockdown of ATF4 causes deficits in synaptic plasticity and LTM[39]. Therefore, using the iPKR system, we achieve a spatiotemporally limited inhibition of general translation initiation that is likely accompanied by translationally regulated transcriptional inhibition of CREB-regulated genes. Notably, ATF4 also acts as a transcriptional inducer for Ppp1r15a (also known as *Gadd34*)[40], whose gene product GADD34 is a key component of eIF2α dephosphorylating complex GADD34–PP1. Thus, the increase in ATF4 constrains the temporal window for eIF2α phosphorylation mediated by ciPSI, thereby enabling a temporally stringent control of translation initiation. To further ascertain the effect of blocking protein synthesis on memory processes, we devised an alternate chemogenetic strategy that does not lead to ATF4 increase by blocking cap-dependent translation initiation in LA CamK2α$^+$ neurons with a knock-in mouse line for expressing tet-dependent synthetic microRNA specific for eIF4E, and injected a cocktail of adeno-associated virus (AAV).CamK2α.Cre and AAV.DIO.tTA into the bilateral LA[41] (Extended Data Fig. 5a) to achieve eIF4E knockdown. eIF4E is a component of the eIF4F complex that binds the 5′ m^{7}GTP cap found on the majority of cellular mRNAs, and the availability of free eIF4E is tightly regulated in mammalian cells by eIF4E-binding proteins such as 4E-BP and CYFIP1 (ref. [16]). Knocking down eIF4E in LA CamK2α$^+$ neurons did not impair learning in the auditory threat conditioning paradigm (Extended Data Fig. 5b), but strongly impaired LTM (Extended Data Fig. 5c,d). Together, the LTM deficit observed using two independent approaches for blocking translation initiation in CamK2α.iPKR and CamK2α.4Ekd, respectively, strongly supports our hypothesis that de novo translation in LA Camk2α$^+$ neurons is necessary for consolidation of long-term threat memories.

Bidirectional control of memory strength by phosphorylation of eIF2α S51 in LA principal neurons. Constitutive heterozygous phosphomutant eIF2α S51A (A/+) mice have enhanced LTM in several memory paradigms including contextual and auditory threat conditioning and conditioned taste aversion[12], indicating that phosphorylation of eIF2α S51 is a malleable constraint on

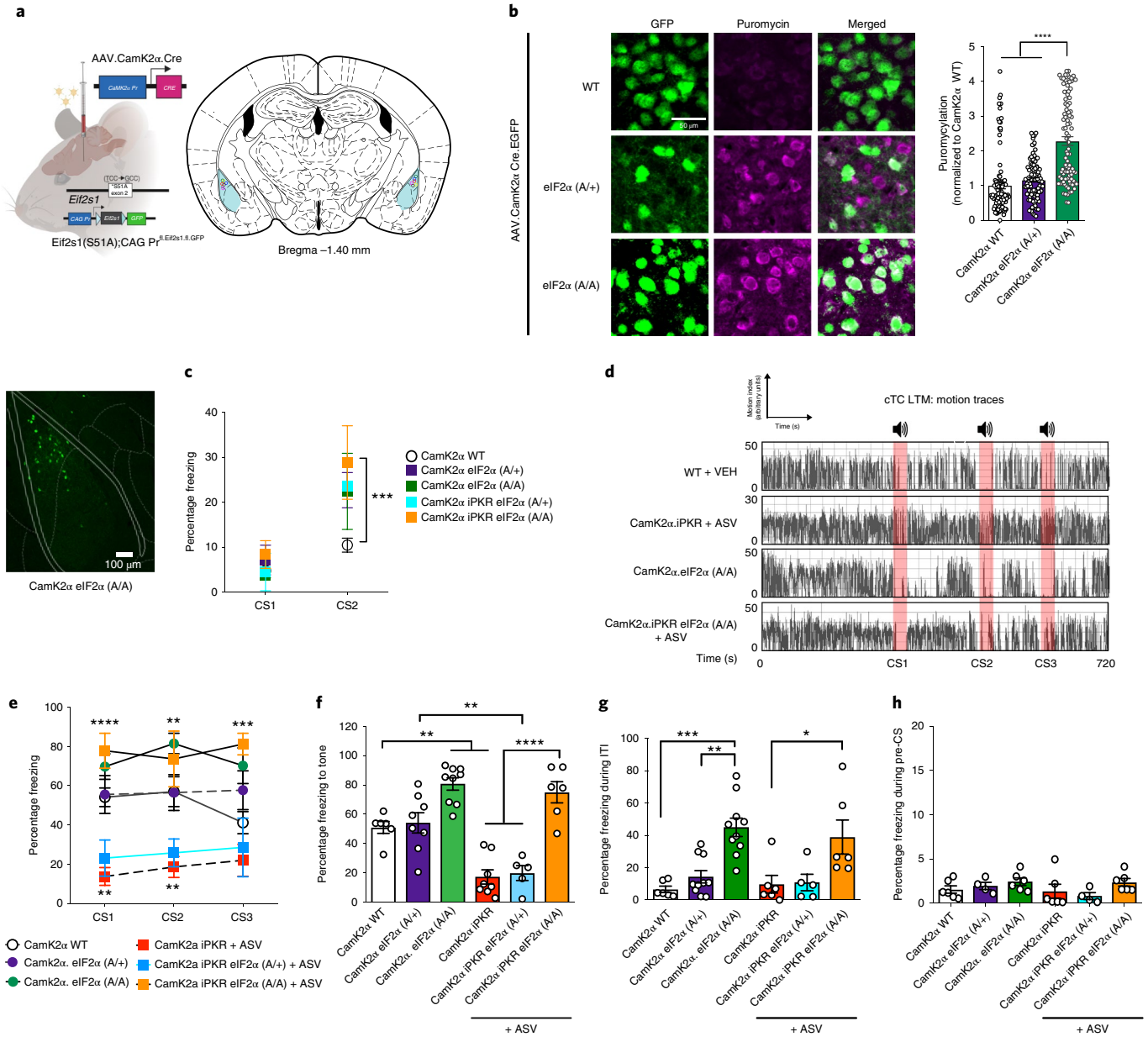

protein synthesis during memory consolidation. Therefore, we virally delivered Camk2α.Cre.eGFP bilaterally to the LA of floxed phosphomutant eIF2α (S51A) mice[42] (Fig. 5a). Targeting phosphomutant eIF2α S51A expression in LA CamK2α$^+$ neurons led to a significant increase in de novo translation in homozygous CamK2α.eIF2α (A/A), but not in heterozygous CamK2α.eIF2α (A/+) neurons, as assessed with in vivo SUnSET (Fig. 5b), and also led to a decrease in p-eIF2α S51 (Extended Data Fig. 6a). Congruently, although all of the mice learned auditory threat conditioning (Fig. 5c), homozygous CamK2α.eIF2α (A/A) mice exhibited significantly higher freezing responses to the conditioned tone in the LTM test, indicating more robust memory compared with WT controls (Fig. 5e,f). We next sought to correct the memory deficit in the CamK2α.iPKR mice by introducing phosphomutant eIF2α, and thus generated CamK2α.iPKR eIF2α (A/+) and CamK2α.iPKR eIF2α (A/A) animals by injecting AAV.CamK2α.Cre in the LA of mice double transgenic for iPKR and eIF2α S51A. Memory deficits in the CamK2a.iPKR mice were completely rescued by dephosphorylating both alleles of eIF2α, but were unaltered by dephosphorylating one allele of eIF2α (Fig. 5e,f). This indicated that the translation tone and LTM consolidation process is set by the phosphorylation of eIF2α, even when the abundance of phosphorylatable eIF2α is reduced by half, and confirmed that the memory deficit caused by iPKR is through the phosphorylation of eIF2α and not due to nonspecific cellular toxicity.

Notably, the memory enhancement in the CamK2α.eIF2α (A/A) mice came with a cost. We found that the dysregulated increase in translation tone in CamK2α.eIF2α (A/A) mice resulted in impaired behavioral flexibility during the tone offset in the LTM test. CamK2α.eIF2α (A/A) mice freeze starting at tone onset but continue to freeze after the tone offset during intertrial interval (ITI) epochs (Extended Data Fig. 6b and Fig. 5g). This failure to switch off defensive state is triggered only after the onset of first tone, whereas at preconditioned stimulus (pre-CS) the animals have normal motor behavior, indicating absence of generalized anxiety or contextual threat response (Fig. 5h). We next tested CamK2α.eIF2α (A/A) animals in open field arena and elevated plus maze, and found normal locomotion in open field (Extended Data Fig. 6c–e), but a decrease in the percentage of time spent in the open arm in the elevated plus maze, indicative of increased anxiety-like behavior (Extended Data Fig. 6f,g). These data suggest that a dysregulated increase in the translation program regulated by eIF2α leads to a failure in risk assessment in nonthreating environments and epochs. These findings also are consistent with the anxiolytic effect of iPKR-mediated eIF2α phosphorylation on exploratory behavior in the open arm of elevated plus maze, and thus support the relevance of an eIF2α-dependent translation program in eliciting anxiety-related behaviors.

Dysregulated protein synthesis in LA CamK2α$^+$ neurons compromises the precision of a complex memory. Finally, we addressed whether lost memories can be rescued with artificial reactivation[43] of LA CamK2α$^+$ principal neurons. Designer drug activated by designer drug (DREADD) hM3Dq-mediated neuronal activation engages the mitogen-activated protein kinase ERK1/2 and mTORC1 pathways that are positively associated with protein synthesis[44,45]. We injected a cocktail of AAV.CamK2α.Cre together with AAV.hSyn.DIO.hM3Dq.mCherry into the LA of iPKR knock-in mice (Fig. 6a). DREADD agonist C21 (ref. [46]) significantly increased de novo translation in CamK2α$^+$ neurons of CamK2α.iPKR hM3Dq mice compared with the vehicle (VEH)-treated group (Fig. 6b). We then trained CamK2α.iPKR hM3Dq, CamK2α.hM3Dq and WT control mice in a differential threat conditioning paradigm that involves three interleaved presentations of a paired tone (CS+) and an unpaired tone (CS−) in a single session (Fig. 6c,d). Consistent with earlier data, posttraining ASV infusion impaired LTM and led to a significant decline in freezing response to paired tone (Fig. 6f,g). Forty-eight hours after LTM1 test, we retested the animals for LTM2 in a different context after chemogenetic activation of hM3Dq receptors in the CamK2α$^+$ neurons using agonist C21. We found that although artificial reactivation of CamK2α$^+$ neurons recovered CS+LTM, it led to stimulus generalization and resulted in generalized defensive freezing response to CS− (Fig. 6h) that reflected in a significant decline in threat discrimination index (Fig. 6i). CamK2α WT and CamK2α.hM3Dq mice exhibited no change in discrimination index between the two LTM tests. Besides stimulus generalization, freezing during ITI was also increased by artificially boosting protein synthesis in translation-inhibited CamK2α$^+$ neurons (Extended Data Fig. 7a,b).

To further understand what happens when eIF2α-controlled general translation in LA principal neurons is boosted during consolidation of a complex memory, we explored differential threat conditioning in CamK2α eIF2α S51A mice (Extended Data Fig. 7c). We found that whereas homozygous CamK2α.eIF2α (A/A) mice can discriminate between CS+ and CS− during LTM, they have a significantly increased freezing response to CS−. In contrast,

Fig. 6 | Artificial reactivation of LA principal neurons compromises the precision of a complex memory. a, CamK2α.iPKR.hM3Dq and CamK2α.hM3Dq mice were generated by bilaterally injecting AAV1.CamK2α.Cre and AAV9.hSyn.DIO.hM3Dq.mCherry into the LA of either iPKR or WT mice. **b**, DREADD receptor agonist C21 significantly enhanced de novo translation, as measured with in vivo SUnSET, in CamK2α.iPKR.hM3Dq neurons compared with VEH treatment (****$P < 0.0001$). Two-tailed unpaired *t*-test was used. *n*(CamK2α.iPKR.hM3Dq+VEH) = 74 neurons from three mice and *n*(CamK2α.iPKR.hM3Dq+ASV) = 82 neurons from three mice. **c**, Schematic of experimental paradigm for cTD conditioning in CamK2α.iPKR.hM3Dq mice. **d**,**e**, CamK2α WT, CamK2α.hM3Dq and CamK2α.iPKR hM3Dq mice learned equivalently to associate CS+ with US during training (**d**), although they did not yet develop discrimination of CS− from CS+ during training (**e**). *n*(CamK2α WT) = 4 animals, *n*(CamK2α.hM3Dq) = 7 animals and *n*(CamK2α.iPKR.hM3Dq) = 7 animals. **f**, Representative cTD LTM motion traces for WT mice, CamK2α.iPKR.hM3Dq mice that were infused with ASV immediately after training and CamK2α.iPKR.hM3Dq mice that underwent reactivation of LA principal neurons with C21 and CamK2α.eIF2α (A/A) mice. **g**, CamK2α.iPKR.hM3Dq mice infused with ASV immediately after training exhibited a significant CS+ memory deficit compared with ASV-treated WT CamK2α.hM3Dq mice (***$P < 0.001$). *n*(CamK2α WT) = 9 animals, *n*(CamK2α.hM3Dq) = 6 animals and *n*(CamK2α.iPKR.hM3Dq+ASV) = 9 animals. One-way ANOVA with Bonferroni's post hoc test was conducted. Genotype–drug–CS interaction: $F(2,44) = 8.30$, $P = 0.0009$; genotype–drug: $F(1,44) = 83.69$, $P = 0.0025$; CS: $F(2,44) = 6.904$, $P < 0.0001$. **h**, Artificial reactivation of LA principal neurons in CamK2α.iPKR.hM3Dq neurons using C21 recovered CS+ LTM (*$P < 0.05$), but caused stimulus generalization to CS− (*$P < 0.05$). *n*(CamK2α WT) = 6 animals, *n*(CamK2α.hM3Dq) = 7 animals and *n*(CamK2α.iPKR.hM3Dq+C21) = 9 animals. One-way ANOVA with Bonferroni's post hoc test. Genotype–drug–CS interaction: $F(2,19) = 6.888$, $P = 0.0056$; CS: $F(1,19) = 55.84$, $P < 0.0001$. **i**, cTD discrimination index was significantly decreased in CamK2α.iPKR.hM3Dq mice that underwent artificial reactivation after ciPSI compared with CamK2α.hM3Dq WT mice (**$P < 0.01$). *n*(CamK2α WT, LTM1) = 6 animals, *n*(CamK2α.hM3Dq, LTM1) = 7 animals, *n*(CamK2α.iPKR.hM3Dq+ASV, LTM1) = 8 animals, *n*(CamK2α WT, LTM2) = 6 animals, *n*(CamK2α.hM3Dq, LTM2) = 7 animals and *n*(CamK2α.iPKR.hM3Dq+C21, LTM2) = 8 animals. Two-way ANOVA with Bonferroni's post hoc test was performed. Genotype: $F(2,36) = 8.604$, $P = 0.0009$; LTM test: $F(1,36) = 6.773$, $P = 0.0134$. Data are presented as mean ± s.e.m. *$P < 0.05$, **$P < 0.01$, ***$P < 0.001$, ****$P < 0.0001$.

CamK2α WT mice robustly discriminated CS+ from CS− and displayed negligible freezing responses to CS− (Extended Data Fig. 7d). The enhanced CS− response in the CamK2α.eIF2α (A/A) mice resulted in a poor discrimination index (Extended Data Fig. 7e). We next examined the freezing during ITI and found that similar to earlier results with simple threat conditioning, CamK2α.eIF2α (A/A) exhibited a significantly increased freezing response after tone offset, indicating behavioral inflexibility (Extended Data Fig. 7f,g). These findings indicate that the precision of a memory trace is contributed by the finely regulated translation program in LA CamK2α$^+$ neurons during memory consolidation.

Discussion

Protein synthesis is metabolically expensive and thus is tightly regulated at the level of initiation, which has limited investigation of cell-autonomous protein synthesis in physiological processes, but until now an effective chemogenetic tool to block protein synthesis has been lacking. To address this issue, we have bioengineered a spatiotemporally precise chemogenetic resource for rapidly and reversibly blocking cell-autonomous protein synthesis via phosphorylation of eIF2α. Phosphorylation of eIF2α is a tightly regulated molecular event that acts as a master effector of the integrated stress response. Using our chemogenetic iPKR mouse resource, we made several notable discoveries. First, temporally structured pan-neuronal protein synthesis is required for LTM consolidation. Recent LTM examined 24 h after training is most sensitive to protein synthesis disruption in the first hour after training. Second, blocking de novo translation in CamK2α$^+$ principal neurons within the LA disrupts LTM consolidation. This block of memory consolidation can be rescued either by using the eIF2B activator ISRIB or

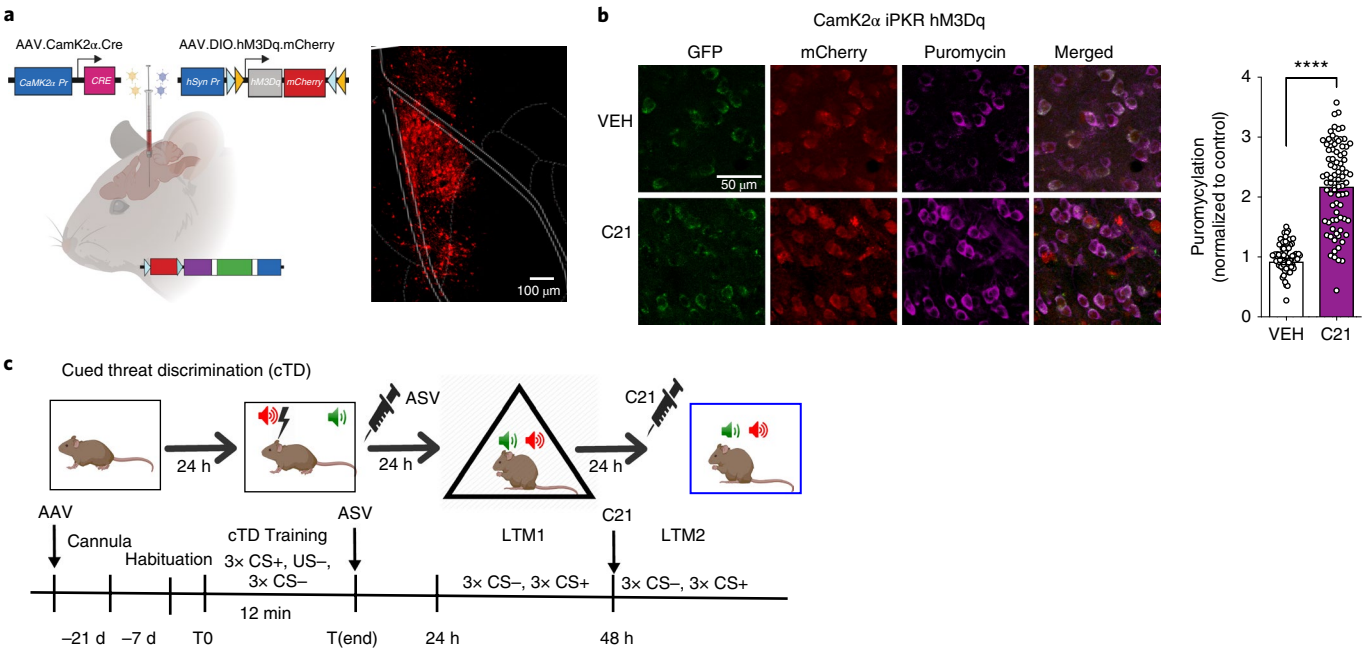

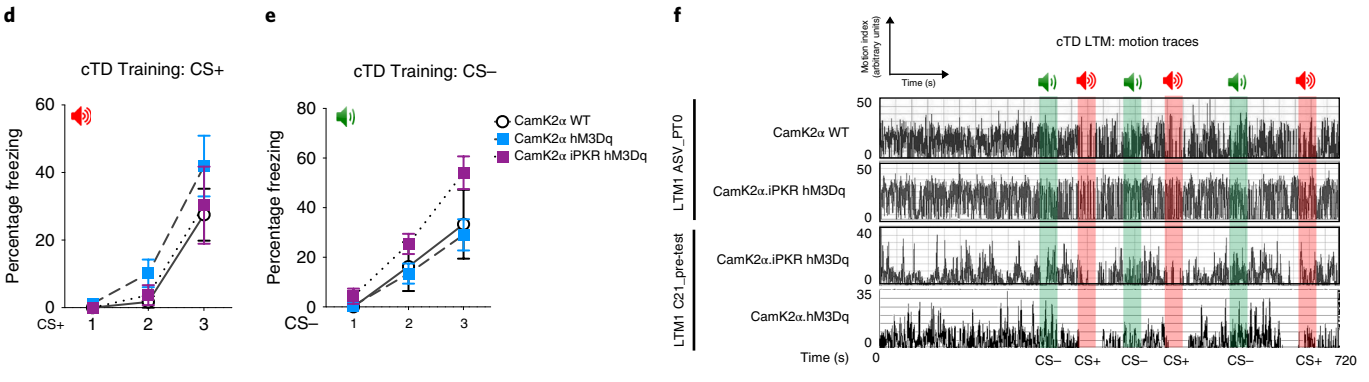

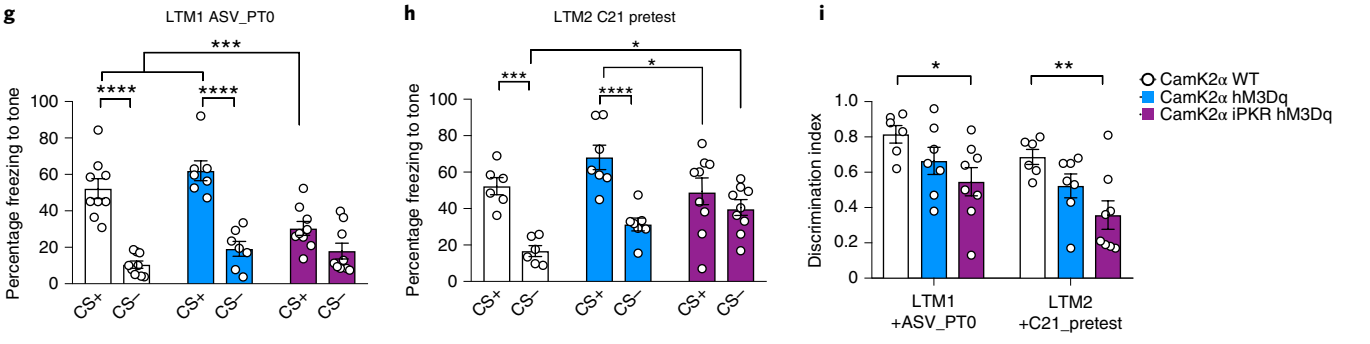

by dephosphorylating both alleles of eIF2α. Third, expressing a biallelic phosphomutant eIF2α in CamK2α$^+$ principal neurons results in enhanced strength of the memory, but introduces behavioral inflexibility and a generalized defensive response for an unpaired or safe tone. Fourth, artificial reactivation of LA CamK2α$^+$ neurons 24 h after protein synthesis inhibition recovers lost memory for the paired tone but causes stimulus generalization.

Protein synthesis dependence during memory consolidation. We found that too little or too much phosphorylation of eIF2α causes aberrant memory storage and expression. A parsimonious interpretation of our data is that state-dependent modulation of eIF2α phosphorylation is critical for a finely tuned translation program supporting the associative memory. eIF2α phosphorylation itself is a homeostatic process wherein the phosphorylation event triggers the synthesis of the eIF2α dephosphorylating enzyme GADD34, bringing the system back to a lower state of eIF2α phosphorylation. Our data are consistent with Batista et al.[47], showing that phosphorylation of eIF2α causes a block of general translation. In contrast, Jiang et al.[13] reported that chemogenetic dimerization of FK506-binding protein (FKBP)-PKR (fPKR) induced phosphorylation of eIF2α by 1.5-fold without blocking general translation; thus, they attributed the memory deficit in fPKR-expressing animals to ATF4 expression. It is possible that because these investigators injected the drug inducer of fPKR (AP20187) 2 h before radioisotope S^{35} methionine injection intraperitoneally, the sensitive time window for protein synthesis disruption was missed during labeling. Compared with fPKR, PKRk is more effective in suppressing translation because it not only directly phosphorylates eIF2α, but it also interacts with and phosphorylates endogenous full-length PKR, further boosting eIF2α S51 phosphorylation[48]. In our system, central infusion of ASV resulted in a 2-fold increase in p-eIF2α, which resulted in a robust 50% decrease of general translation as assessed with in vivo SUnSET that involved local infusion of puromycin directly into the LA. Our convergent data from a parallel strategy of cell-autonomous protein synthesis inhibition in LA CamK2α$^+$ neurons using a synthetic microRNA against eIF4E provides further support for the requirement of de novo protein synthesis in LTM consolidation. Nonetheless, we also observed an increase in ATF4 levels after phosphorylation of eIF2α and cannot exclude the possibility that the memory deficit in the iPKR transgenic mice is in part due to upregulated translation of transcripts containing uORFs, such as ATF4, and the ensuing repression of CREB-regulated genes.

Memory generalization and behavioral inflexibility as a result of dysregulated translation. Several studies have used immediate early gene-based engram cell targeting approaches to interrogate the nature of memory formation and recall. Artificial reactivation of conditioned threat engram cells in the LA using optogenetics has been shown to recover memories previously lost by protein synthesis inhibition using anisomycin[49,50]. Our chemogenetic iPKR mouse resource is not amenable for the engram cell targeting approach because the engram cells by definition need to be tagged during the training event for iPKR expression, a process dependent on de novo transcription and translation. Nonetheless, our results show that artificial reactivation of previously translation-inhibited CamK2α$^+$ neurons in the LA results in memory recovery, but at the cost of stimulus generalization. We propose that learning-induced somatic and synaptic protein synthesis functions to stabilize the connections between the pathway-specific afferents from conditioned tone processing brain regions (auditory cortex and auditory thalamus) to amygdalar engram cells in such a way that the conditioned tone can access and activate the downstream neuronal network in the LA during recall. This natural cue-elicited neuronal reactivation is incompletely recapitulated by artificial reactivation of LA neurons, such that there is imprecise restoration of the memory, perhaps because of a lack of reinstatement of synapse specificity of the original memory trace. Phosphomutant eIF2α mice, with a rigid increase in translation in LA principal neurons, also exhibit stimulus generalization and behavioral inflexibility at tone offset. Taken together, our data indicate that a finely tuned translation program in the amygdala is required to coordinate the stability and precision of the LTM trace.

Model of protein synthesis regulation during LTM consolidation. Based on our data, we propose the following cellular/molecular model of protein synthesis regulation in the LA during long-term consolidation. cTC leads to a coordinated increase in protein synthesis in CamK2α$^+$ neurons in the soma and in local subcellular compartments, such as dendritic spines and axons. This results in robust memory strength and precision (Extended Data Fig. 8a). Chemogenetic inhibition of protein synthesis using iPKR blocks general translation in LA CamK2α$^+$ neurons, resulting in memory loss (Extended Data Fig. 8b). Expression of biallelic phosphomutant eIF2α in LA CamK2α$^+$ neurons, although insensitive to iPKR-mediated eIF2α phosphorylation, results in an aberrant increase in basal translation. This leads to robust memory strength, but low memory precision (Extended Data Fig. 8c). Artificial chemogenetic reactivation of CamK2α$^+$ neurons following inhibition of protein synthesis leads to an increase in protein synthesis but does not recapitulate learning-induced local translation, thus causing memory generalization. This is manifested as normalized memory strength and low memory precision (Extended Data Fig. 8d).

We have used multipronged chemogenetic approaches to investigate the translational control of long-term threat memories. Future studies will be required to elucidate how protein synthesis regulation occurs in genetically defined and functionally coherent cell types within the memory network during LTM consolidation.

Online content

Any methods, additional references, Nature Research reporting summaries, source data, extended data, supplementary information, acknowledgements, peer review information; details of author contributions and competing interests; and statements of data and code availability are available at https://doi.org/10.1038/s41593-019-0568-z.

Received: 3 June 2019; Accepted: 5 December 2019;
Published online: 20 January 2020

References

1. Tovote, P., Fadok, J. P. & Luthi, A. Neuronal circuits for fear and anxiety. *Nat. Rev. Neurosci.* **16**, 317–31 (2015).
2. Wheeler, A. L. et al. Identification of a functional connectome for long term fear memory in mice. *PLoS Comput. Biol.* **9**, e1002853 (2013).
3. Clugnet, M. C. & LeDoux, J. E. Synaptic plasticity in fear conditioning circuits: induction of LTP in lateral nucleus of the amygdala by stimulation of the medial geniculate body. *J. Neurosci.* **10**, 2818–2824 (1990).
4. Maren, S., Ferrario, C. R., Corcoran, K. A., Desmond, T. J. & Frey, K. A. Protein synthesis in the amygdala, but not the auditory thalamus, is required for consolidation of Pavlovian fear conditioning in rats. *Eur. J. Neurosci.* **18**, 3080–3088 (2003).
5. Flexner, L. B., Flexner, J. B., Roberts, R. B. & Delahaba, G. Loss of recent memory in mice as related to regional inhibition of cerebral protein synthesis. *Proc. Natl Acad. Sci. USA* **52**, 1165–1169 (1964).
6. Davis, H. P. & Squire, L. R. Protein synthesis and memory: a review. *Psychol. Bull.* **96**, 518–559 (1984).
7. Bourtchouladze, R. et al. Different training procedures recruit either one or two critical periods for contextual memory consolidation, each of which requires protein synthesis and PKA. *Learn. Mem.* **5**, 365–374 (1998).
8. Hoeffer, C. A. et al. Inhibition of the interactions between eukaryotic initiation factors 4E and 4G impairs long-term associative memory consolidation but not reconsolidation. *Proc. Natl Acad. Sci. USA* **108**, 3383–3388 (2011).
9. Qi, Z. & Gold, P. E. Intrahippocampal infusions of anisomycin produce amnesia: contribution of increased release of norepinephrine, dopamine and acetylcholine. *Learn. Mem.* **16**, 308–314 (2009).

10. Radulovic, J. & Tronson, N. C. Protein synthesis inhibitors, gene superinduction and memory: too little or too much protein? *Neurobiol. Learn. Mem.* **89**, 212–218 (2008).
11. Banko, J. L. et al. The translation repressor 4E-BP2 is critical for eIF4F complex formation, synaptic plasticity, and memory in the hippocampus. *J. Neurosci.* **25**, 9581–9590 (2005).
12. Costa-Mattioli, M. et al. eIF2alpha phosphorylation bidirectionally regulates the switch from short- to long-term synaptic plasticity and memory. *Cell* **129**, 195–206 (2007).
13. Jiang, Z. et al. eIF2alpha phosphorylation-dependent translation in CA1 pyramidal cells impairs hippocampal memory consolidation without affecting general translation. *J. Neurosci.* **30**, 2582–2594 (2010).
14. Heumeller, M. et al. A genetically encodable cell type-specific protein synthesis inhibitor. *Nat. Methods* **16**, 699–702 (2019).
15. Klann, E. & Dever, T. E. Biochemical mechanisms for translational regulation in synaptic plasticity. *Nat. Rev. Neurosci.* **5**, 931–942 (2004).
16. Sonenberg, N. & Hinnebusch, A. G. Regulation of translation initiation in eukaryotes: mechanisms and biological targets. *Cell* **136**, 731–745 (2009).
17. Takei, N., Kawamura, M., Hara, K., Yonezawa, K. & Nawa, H. Brain-derived neurotrophic factor enhances neuronal translation by activating multiple initiation processes: comparison with the effects of insulin. *J. Biol. Chem.* **276**, 42818–42825 (2001).
18. Flores, M. V., Strawbridge, J., Ciaramella, G. & Corbau, R. HCV-NS3 inhibitors: determination of their kinetic parameters and mechanism. *Biochim. Biophys. Acta* **1794**, 1441–1448 (2009).
19. Gentile, I. et al. Asunaprevir, a protease inhibitor for the treatment of hepatitis C infection. *Ther. Clin. Risk Manag.* **10**, 493–504 (2014).
20. Saelens, X., Kalai, M. & Vandenabeele, P. Translation inhibition in apoptosis. *J. Biol. Chem.* **276**, 41620–41628 (2001).
21. Butko, M. T. et al. Fluorescent and photo-oxidizing TimeSTAMP tags track protein fates in light and electron microscopy. *Nat. Neurosci.* **15**, 1742–1751 (2012).
22. Donnelly, M. L. et al. The 'cleavage' activities of foot-and-mouth disease virus 2A site directed mutants and natually occuring '2A-like' sequences. *J. Gen. Virol.* **82**(Pt 5), 1027–1041 (2001).
23. Klinakis, A. et al. Igf1r as a therapeutic target in a mouse model of basal-like breast cancer. *Proc. Natl Acad. Sci. USA* **106**, 2359–2364 (2009).
24. Doyle, J. P. et al. Application of a translational profiling approach for the comparative analysis of CNS cell types. *Cell* **135**, 749–762 (2008).
25. Tronche, F. et al. Disruption of the glucocorticoid receptor gene in the nervous system results in reduced anxiety. *Nat. Genet.* **23**, 99–103 (1999).
26. Dieterich, D. C. et al. Labeling, detection and identification of newly synthesized proteomes with bioorthogonal non-canonical amino-acid tagging. *Nat. Protoc.* **2**, 532–540 (2007).
27. Schmidt, E. K., Clavarino, G., Ceppi, M. & Pierre, P. SUnSET, a nonradioactive method to monitor protein synthesis. *Nat. Methods* **6**, 275–277 (2009).
28. Huang, Y.-Y., Martin, K. C. & Kandel, E. R. Both protein kinase A and mitogen-activated protein kinase are required in the amygdala for the macromolecular synthesis-dependent late phase of long-term potentiation. *J. Neurosci.* **20**, 6317–6325 (2000).
29. Johnson, L. R. et al. A recurrent network in the lateral amygdala: a mechanism for coincidence detection. *Front. Neural Circuits* **2**, 3 (2008).
30. Costa-Mattioli, M. et al. Translational control of hippocampal synaptic plasticity and memory by the eIF2alpha kinase GCN2. *Nature* **436**, 1166–1173 (2005).
31. Zhu, P. J. et al. Suppression of PKR promotes network excitability and enhanced cognition by interferon mediated disinhibition. *Cell* **147**, 1384–1396 (2011).
32. Stern, E., Chinnakkaruppan, A., David, O., Sonenberg, N. & Rosenblum, K. Blocking the eIF2alpha kinase (PKR) enhances positive and negative forms of cortex dependent taste memory. *J. Neurosci.* **33**, 2517–2525 (2013).
33. Igaz, L. M., Vianna, M. R., Medina, J. H. & Izquierdo, I. Two time periods of hippocampal mRNA synthesis are required for memory consolidation of fear motivated learning. *J. Neurosci.* **22**, 6781–6789 (2002).
34. Wilensky, A. E., Schafe, G. E. & LeDoux, J. E. Functional inactivation of the amygdala before but not after auditory fear conditioning prevents memory formation. *J. Neurosci.* **19**, RC48 (1999).
35. Quirk, G. J., Repa, C. & LeDoux, J. E. Fear conditioning enhances short-latency auditory responses of lateral amygdala neurons: parallel recordings in the freely behaving rat. *Neuron* **15**, 1029–1039 (1995).
36. Schafe, G. E. & Ledoux, J. E. Memory consolidation of auditory pavlovian fear conditioning requires protein synthesis and protein kinase A in the amygdala. *J. Neurosci.* **20**, RC96 (2000).
37. Rogan, M. T., Staubli, U. V. & LeDoux, J. E. Fear conditioning induces associative long-term potentiation in the amygdala. *Nature* **390**, 604–607 (1997).
38. Sidrauski, C., McGeachy, A. M., Ingolia, N. T. & Walter, P. The small molecule ISRIB reverses the effects of eIF2α phosporylation on translation and stress granule assembly. *eLife* **4**, e05033 (2015).
39. Pasini, S., Corona, C., Liu, J., Greene, L. A. & Shelanski, M. L. Specific downregulation of hippocampal ATF4 reveals a necessary role in synaptic plasticity and memory. *Cell Rep.* **11**, 183–191 (2015).
40. Ma, Y. & Hendershot, L. M. Delineation of a negative feedback regulatory loop that controls protein translation during endoplasmic reticulum stress. *J. Biol. Chem.* **278**, 34864–34873 (2003).
41. Lin, C.-J. et al. Targeting synthetic lethal interactions between Myc and the eIF4F complex impedes tumorigenesis. *Cell Rep.* **1**, 325–333 (2012).
42. Back, S. H. et al. Translation attenuation through eIF2α phosphorylation prevents oxidative stress and maintains the differentiated state in beta cells. *Cell Metab.* **10**, 13–26 (2009).
43. Shrestha, P. & Klann, E. Lost memories found. *Nature* **531**, 450–451 (2016).
44. Ambruster, B. N., Li, X., Pausch, M. H., Herlitze, S. & Roth, B. L. Evolving the lock to fit the key to create a family of G protein-coupled receptors potently activated by an inert ligand. *Proc. Natl Acad. Sci. USA* **104**, 5163–5168 (2007).
45. Li, S. et al. Promoting axon regeneration in the adult CNS by modulation of the melanopsin/GPCR signaling. *Proc. Natl Acad. Sci. USA* **113**, 1937–1942 (2016).
46. Thompson, K. J. et al. DREADD agonist 21 (C21) is an effective agonist for muscarinic-based DREADDs in vitro and in vivo. *ACS Pharmacol. Transl. Sci.* **1**, 61–72 (2018).
47. Batista, G. et al. Translational control of auditory imprinting and structural plasticity by eIF2α. *eLife* **2016**, e17197 (2016).
48. Kalai, M. et al. The caspase-generated fragment of PKR cooperate to activate full-length PKR and inhibit translation. *Cell Death Differ.* **14**, 1050–1059 (2007).
49. Abdou, K. et al. Synapse-specific representation of the identity of overlapping memory engrams. *Science* **360**, 1227–1231 (2018).
50. Ryan, T. J., Roy, D. S., Pignatelli, M., Arons, A. & Tonegawa, S. Engram cells retain memory under retrograde amnesia. *Science* **348**, 1007–1013 (2015).

Publisher's note Springer Nature remains neutral with regard to jurisdictional claims in published maps and institutional affiliations.

© The Author(s), under exclusive licence to Springer Nature America, Inc. 2020

Methods

Cloning of recombinant plasmids. iPKR was produced by adding the NS5A/B junction sequence (DEMEECASHLPY) within the PKRk. NS3/4 protease, iPKR and GFP were amplified using Phusion polymerase (NEB) and cloned into p-eGFP-N1 vector (Clontech) using appropriate restriction enzymes (NEB). All constructs were verified by sequencing. Purifications were done using a PCR extraction kit (Qiagen). The ligations were performed with Quick Ligase kit (NEB), and the products were transformed into chemically competent TOP10 cells (Invitrogen) that were grown in Luria–Bertani medium containing 35 mg ml^{-1} kanamycin (Sigma). The mammalian expression constructs were subcloned into the gene-targeting plasmids as previously reported[31]. The final construct was extracted with phenol:chloroform:isoamyl alcohol (25:24:1), precipitated in 70% ethanol and dissolved in Tris–EDTA buffer.

Cell culture and transfection. 293T cells were grown in a 24-well plate in growth medium (Invitrogen) supplemented with 10% fetal bovine serum (Invitrogen) to have 90% confluency on the day of transfection. Transfection was carried out with 1 µg of a reference plasmid using 2 µl 293fectin reagent (Invitrogen). The amounts of the remaining plasmids were adjusted to have the same molarity per well. Cells were lysed on ice in phosphate-buffered saline supplied with 1% Triton X-100 (Sigma) and inhibitors against proteases (78437; Pierce), phosphatases (78420; Pierce) and translation machinery (100 µg ml^{-1} cycloheximide; Sigma); the cytosolic extracts were isolated after precipitating the insoluble fraction. The protein concentrations were measured using bicinchoninic acid protein assay (Pierce).

Generation of iPKR knock-in animals. 129S6/SvEvTac embryonic stem cells of the W4 parental cell line were used for homologous recombination at *Eef1a1* genomic locus. Gene targeting, generation of knock-in mice and Southern blotting were conducted by the Gene Targeting Facility at The Rockefeller University (New York, NY, USA), as previously described[14]. The following primers were used for genotyping: β-actin forward, 5′-GGC TGT ATT CCC CTC CAT CG-3′ and β-actin reverse, 5′-CCA GTT GGT AAC AAT GCC ATG T-3′; eGFP forward, 5′-GCA GAA GAA CGG CAT CAA GGT-3′ and eGFP reverse, 5′-ACG AAC TCC AGC AGG ACC ATG-3′; iPKR forward, 5′-CAC CAT GGG CAA GCC CCA GCG TCT GTA TG-3′ and iPKR reverse, 5′-TGC CGG TCC AGG TGT AGC TCA TGC TGC AGC-3′.

Animals. Mice were provided with food and water ad libitum and were maintained in a 12–12 h light–dark cycle at New York University at stable temperature (78 °F) and humidity (40–50%). All mice were backcrossed to the C57Bl/6J strain for at least five generations. Nestin Cre transgenic mice (stock no. 003771) were obtained from Jackson laboratory as previously described[25]. Nestin Cre mice were bred to the floxed iPKR knock-in mouse line to generate transheterozygote Nes.iPKR mice. Transgenic homozygous Eif2s1 (S51A); CAG Pr$^{fl.Eif2s1.fl.GFP}$ mice (that is, eIF2α (A/A)) were a gift from Dr Randal Kaufman. Double-transgenic floxed iPKR/eIF2α (A/A) or (A/+) mice were obtained by breeding floxed iPKR mice with eIF2α (A/A) mice. Col1a1$^{TRE\ GFP.shmir4E.389}$ mice were a gift from Dr Jerry Pelletier. Both male and female mice were used for all experiments; no sex-specific differences were noted in any measure. Mice tested in behavioral assays were 10–15 weeks old. All procedures involving the use of animals were performed in accordance with the guidelines of the National Institutes of Health and were approved by the University Animal Welfare Committee of New York University.

Drugs and chemicals. ASV (ChemExpress) was dissolved in dimethylsulfoxide (DMSO) for a stock concentration of 10 mM and diluted in sterile saline to 100 nM. Two microliters of this drug was intracranially infused into the left lateral ventricle (−0.50 mm anteroposterior (AP), −1.10 mm mediolateral (ML) and −2.20 mm dorsoventral (DV)) using an injection cannula inserted into the stainless steel guide cannula (Plastics One). Except for the dosage curve experiments, 100 nM ASV was used in all experiments involving protein synthesis inhibition in vivo. ASV infusion was carried out at 0.5 µl min^{-1} using an injection cannula extending out of PE50 tubing attached to a 5-µl Hamilton syringe (Hamilton) using a PHD 2000 Infusion Pump (Harvard Apparatus). After injection, the injection cannula was kept in place for 1 min before its withdrawal. Puromycin (P8833; Sigma) was dissolved in double-distilled H_2O at 25 µg µl^{-1}, and this stock was freshly diluted in saline for SUnSET assays in vivo. For SUnSET immunoblot, 2 µl of 25 µg µl^{-1} puromycin was infused into the lateral ventricle. For SUnSET immunohistochemistry, 0.5 µl of 10 µg µl^{-1} puromycin was infused into the LA (−1.40 mm AP, −3.50 mm ML and −4.60 mm DV) of awake behaving mice using internal cannula with 1-mm projection. For BONCAT ex vivo assays, AHA (NC0667352; Fisher) was dissolved in distilled water at 100 mM. A total of 1 mM AHA was bath applied to amygdala slices in artificial cerebrospinal fluid (aCSF; 125 mM NaCl, 2.5 mM KCl, 1.25 mM NaH_2PO_4, 25 mM $NaHCO_3$, 25 mM glucose, 1 mM $MgCl_2$ and 2 mM $CaCl_2$). DREADD actuator, agonist C21 (Tocris), was dissolved in DMSO at 40 mg ml^{-1} concentration, freshly diluted in saline and administered to mice at 1 mg kg^{-1} intraperitoneally. A total of 25 mM PKR inhibitor C16 (Calbiochem) was dissolved in DMSO and diluted in saline to a final DMSO concentration of 0.5%. PKR inhibitor C16 was administered intraperitoneally at a 5 mg kg^{-1} dosage 30 min before training when specified. ISRIB was dissolved in 1:1 PEG400:DMSO and injected in mice at 2.5 mg kg^{-1} intraperitoneally as previously described[38]. Doxycycline was prepared in rodent chow (Bio-Serv) at 40 mg kg^{-1}, and this diet was provided to the mice in the 4Ekd group for 2 weeks after surgery.

Stereotaxic surgeries. Mice were anesthetized with the mixture of ketamine (100 mg kg^{-1}) and xylazine (10 mg kg^{-1}) in saline (intraperitoneal injection). To generate CamK2α.iPKR mice designated for behavior testing, we injected 100 nl AAV1.Camk2α.Cre (1.6×10^{13} genome copies (GCs) per ml; UPenn Vector Core) bilaterally into the LA (−1.40 mm AP, ±3.50 mm ML and −4.60 mm DV) of iPKR mice. Two weeks after viral injections, CamK2α.iPKR mice underwent a second surgery for implantation of 23 gauge stainless steel guide cannulas (Plastics One) in the left lateral ventricle (−0.50 mm AP, −1.10 mm ML and −2.20 DV). One skull screw was inserted into the skull, and dental cement was applied to secure the cannula in position (Parkell and Stoelting). For in vivo SUnSET immunohistochemistry, CamK2α.iPKR mice were implanted with two guide cannulas, one in the lateral ventricle (−0.50 mm AP, −1.10 mm ML and −2.20 DV) for ASV infusion and a second one in the LA (−1.40 mm AP, +3.50 mm ML and −3.60 mm DV) for puromycin infusion. For assessing phosphorylation of eIF2α S51, a separate group of CamK2α GFP.iPKR mice was generated by injecting AAV9.Camk2α.Cre.eGFP and AAV9.DIO.tTA in the LA. For eIF4E knockdown experiments, 100 nl each of AAV1.Camk2α.Cre and AAV9.CAG.DIO.tTA (1×10^{13} GCs per ml; Vigene) was injected into the LA of Col1a1$^{TRE\ GFP.shmir4E.389}$ mice. Control WT littermates were injected with 100 nl each of AAV1.Camk2α.Cre and AAV9.CAG.DIO.GFP (3.33×10^{13} GCs per ml; UPenn Vector Core). For artificial reactivation studies involving CamK2α.iPKR hM3Dq mice, a mixture of 100 nl each of AAV1.Camk2α.Cre and AAV.hSyn Pr.DIO. hM3Dq.mCherry (2.31×10^{12} GCs per ml; Addgene) was injected bilaterally into the LA of iPKR mice. To generate CamK2α.eIF2α (A/+) and CamK2α.eIF2α (A/A) mice, we injected 100 nl AAV1.Camk2α.Cre (UPenn Vector Core) bilaterally into the LA (−1.40 mm AP, ±−3.50 mm ML and −4.60 mm DV) of eIF2α (A/+) or eIF2α (A/A) mice, respectively. Finally, CamK2α.iPKR eIF2α (A/+) and (A/A) mice were generated by injecting 100 nl AAV1.Camk2α.CRE into the LA (−1.40 mm AP, ±−3.50 mm ML and −4.60 mm DV) of double-transgenic floxed iPKR and eIF2α (A/+) or eIF2α (A/A) mice, respectively. Control WT littermates were injected with AAV9.Camk2α.Cre.eGFP.

Electrophysiology. The electrophysiology experiments were performed as previously described,[27,51] and mice were between 2 and 4 months of age at the time of the experiments. In brief, transverse slices (300 µm) containing the amygdala were isolated and transferred to recording chambers (preheated to 32 °C), where they were superfused with oxygenated aCSF (125 mM NaCl, 2.5 mM KCl, 1.25 mM NaH_2PO_4, 25 mM $NaHCO_3$, 25 mM D-glucose, 2 mM $CaCl_2$ and 1 mM $MgCl_2$) at least 1 h before recordings began at a rate of 2 ml min^{-1}. In most of the experiments, picrotoxin (75 µM; Tocris) was present in the perfusion solution. For bath application, the drugs were made and stored as concentrated stock solutions and diluted 1,000-fold when applied to the perfusate. fEPSPs from the internal capsule pathway were recorded using microelectrodes filled with aCSF (resistance 1–4 MΩ). A bipolar Teflon-coated platinum electrode was placed in the thalamic afferent fiber to the LA, which is located in the ventral part of the striatum just above the central nucleus of the amygdala. The test stimuli for basal synaptic response were at 0.05 Hz. In all experiments, basal fEPSPs were stable for at least 20 min before the start of each experiment. L-LTP was induced with three 1-s 100-Hz HFS trains, with an intertrain interval of 60 s. After induction of L-LTP, we collected fEPSPs for an additional 120 min. A total of 5 nM ASV or VEH was bath applied 10 min before L-LTP induction and lasted for all of the recording. Slope values were compared from the Nes.iPKR transgenic mice, and their control littermates were treated with either ASV or VEH. Synaptic efficacy was monitored at 0.05 Hz and averaged every 2 min. fEPSPs were amplified and digitized using the A-M Systems Model 1800 and Digidata 1440 (Molecular Devices).

Behavior. All behavior sessions were conducted during the light cycle. Mice were randomly assigned for experimental conditions including drug or VEH infusions and for the order of testing in any given experimental paradigm. All behavior data were collected by experimenters blind to the genotype and experimental conditions.

Open field activity. Mice were placed in the center of an open field ($27.31 \times 27.31 \times 20.32$ cm^3) for 15 min during which a computer-operated optical system (Activity monitor software 6.02; Med Associates) monitored the spontaneous movement of the animals as they explored the arena. The parameters tested were distance traveled and the ratio of center to total distance at three epochs.

Elevated plus maze. The plus maze consisted of two open arms (30×5 cm^2) and two enclosed arms of the same size with 14-cm-high sidewalls and an endwall. The arms extended from a common central square (5×5 cm^2) perpendicular to each other, making the shape of a plus sign. The entire plus maze apparatus was elevated to a height of 30 cm. Testing began by placing an animal on the central platform

of the maze facing the open arm. Standard 5-min test duration was applied, and the maze was wiped with 30% ethanol in between trials. Ethovision XT13 software (Noldus) was used to record the time spent on open arms and closed arms, total distance moved, and number of open arm and closed arm entries.

Cued threat conditioning. Mice were habituated for 15 min in the threat conditioning chambers housed inside sound attenuated cubicles (Coulbourn Instruments) for 2 d. The habituation and training context included metal grid floor and white house light. For simple threat conditioning, mice were placed in the context for 270 s and then presented twice with a 5-kHz, 85-dB pure tone for 30 s that coterminated with a 2-s 0.5-mA footshock. The ITI was 2 min and after the second tone shock presentation, mice remained in the chamber for an additional 120 s. cTC LTM was tested 24 h after training in a specific context (context B: vanilla-scented cellulose bedding, white plexiglas platform and red house light) with three presentations of paired tone (CS). STM was tested 1 h after training in a different context (context C: textured blue rubber platform, peppermint odor) with a single presentation of CS. For differential threat conditioning, mice were placed in the training context for 270 s and then trained with interleaved presentations of three paired tones or CS+ (7.5-kHz pulse, 50% duty cycle) that coterminate with 0.5 mA footshock and three unpaired tones or CS− (3-kHz pure tone) in the training context with variable ITI. After the last CS− tone, mice remained in the context for an additional 140 s. The following day, mice were placed in context B for 250 s and cued threat discrimination (cTD) LTM was tested with three interleaved presentations of CS+ and CS− tones with the order reversed from the training day and with variable ITIs. Freezing behavior was automatically measured by Freeze Frame 4 software (ActiMetrics) and manually rescored and verified by an experimenter blind to the genotype/drug.

Western immunoblotting. Mice were euthanized by cervical dislocation. Brain slices 300 µm thick containing amygdala (bregma −1.22 to −2.06 mm) were prepared in cold (4 °C) carbo-oxygenated (95% O_2, 5% CO_2) cutting solution (110 mM sucrose, 60 mM NaCl, 3 mM KCl, 1.25 mM NaH_2PO_4, 28 mM $NaHCO_3$, 5 mM glucose, 0.6 mM ascorbate, 7 mM $MgCl_2$ and 0.5 mM $CaCl_2$) using a VT1200S vibratome (Leica). Amygdala was microdissected from the brain slices and sonicated in ice-cold homogenization buffer (10 mM HEPES, 150 mM NaCl, 50 mM NaF, 1 mM EDTA, 1 mM EGTA, 10 mM $Na_4P_2O_7$, 1% Triton X-100, 0.1% SDS and 10% glycerol) that was freshly supplemented with 10 µl each of protease inhibitor (Sigma) and phosphatase inhibitor (Sigma) per milliliter of homogenization buffer. Protein concentrations were measured using bicinchoninic acid assay (GE Healthcare). Samples were prepared with 5× sample buffer (0.25 M Tris–HCl, pH 6.8, 10% SDS, 0.05% bromophenol blue, 50% glycerol and 25% β-mercaptoethanol) and heat denatured at 95 °C for 5 min. Forty micrograms of protein per lane was run in precast 4–12% Bis–Tris gels (Invitrogen) and subjected to SDS–PAGE followed by wet gel transfer to polyvinylidene difluoride membranes. After blocking in 5% nonfat dry milk in 0.1 M PBS with 0.1% Tween 20 (PBST), membranes were probed overnight at 4 °C using primary antibodies (goat anti-biotin (ab53494, 1:500; Abcam), rabbit anti-p-eIF2α S51 (Cell Signaling 9721, 1:300), rabbit anti-t-eIF2α (9722, 1:500; Cell Signaling), rabbit anti-PKR (ab32506 (Abcam), 3072 (Cell Signaling), 1:300), rabbit ATF4 (sc-390063, 1:300; Santa Cruz), rabbit anti-p-ERK1/2 Thr202/Tyr204 (9101, 1:1,000; Cell Signaling), rabbit anti-ERK1/2 (9102, 1:1,000; Cell Signaling), rabbit anti-p-S6 Ser240/Ser244 (5364, 1:500; Cell Signaling), mouse anti-S6 (2317, 1:500; Cell Signaling), mouse anti-puromycin (MABE343, 1:1,000; Millipore), rabbit anti-Gadd34 (10449-1-AP, 1:1,000; Proteintech), mouse anti-β-tubulin (T8328, 1:5,000; Sigma) and mouse anti-β-actin (A1978, 1:5,000; Sigma). After washing three times in 0.1% PBST, membranes were probed with horseradish peroxidase-conjugated secondary IgG (1:5,000; Promega) for 1 h at room temperature. Signals from membranes were detected with ECL chemiluminescence (Thermo Pierce) using Alpha Imager 3.4 software and the Protein Simple instrument. Exposures were set to obtain signals at the linear range and then normalized by total protein and quantified via densitometry using ImageJ software.

Metabolic labeling in vitro. To visualize the inhibition of protein synthesis, we conducted metabolic labeling experiments. Twenty hours posttransfection with 5 µg iPKR construct (with or without NS3/4 A) and 10 µL reagent, cells in a six-well plate were labeled with 10 µCi TRAN^{35}S label (MP Biomedicals) for 30 min after 30 min of starvation before the addition of the label into L-methionine and L-cysteine-free DMEM media (Invitrogen). Equal amounts of protein from extracts were separated by electrophoresis and transferred on a polyvinylidene difluoride membrane. The membrane was dried in 100% methanol and analyzed for autoradiography; later it was blotted with antibodies and finally stained with Coomassie Plus stain (Pierce).

BONCAT ex vivo. Brain slices containing amygdala were prepared as described earlier and equilibrated in carbo-oxygenated 1:1 cutting solution: aCSF (125 mM NaCl, 2.5 mM KCl, 1.25 mM NaH_2PO_4, 25 mM $NaHCO_3$, 25 mM glucose, 1 mM $MgCl_2$ and 2 mM $CaCl_2$) for 20 min. Brain slices were further allowed to recover in aCSF at 31.2 °C for 45 min, which was then supplemented with 1 mM AHA and either 1 µM ASV or VEH for 3 h. The amygdala then was microdissected and stored at −80 °C until ready for sonication in chelator-free lysis buffer (10 mM HEPES, 150 mM NaCl, 10 mM $Na4P_2O_7$ and 1% SDS) supplemented with 20 µl each of protease and phosphatase inhibitors per milliliter of lysis buffer. A total of 80 µg AHA-tagged protein lysate was subjected to cyclo addition using Protein Reaction Buffer kit with biotin alkyne following the manufacturer's instructions (Life Technologies). Samples were prepared with 5× sample buffer and subjected to immunoblots with anti-biotin.

Surface labeling of translation in vivo. For SUnSET in vivo immunoblotting, Nes.iPKR mice were sequentially infused intracerebroventricularly (i.c.v.) with 150 pg ASV (2 µl, 100 nM) infusion followed 15 min later with 25 µg puromycin. Brain slices were prepared as described earlier in cutting solution, and the amygdala was microdissected and stored at −80 °C until ready for homogenization in lysis buffer (10 mM HEPES, 150 mM NaCl, 50 mM NaF, 1 mM EDTA, 1 mM EGTA, 10 mM $Na_4P_2O_7$, 1% Triton X-100, 0.1% SDS and 10% glycerol). A total of 40 µg puromycylated protein lysate was subjected to western blots with anti-puromycin. For SUnSET in vivo immunohistochemistry, CamK2α.iPKR mice were infused sequentially with ASV (2 µl, 100 nM) i.c.v. followed 15 min later with puromycin (0.5 µl, 10 µg µl^{-1}) in the LA. One hour after puromycin infusion, animals were transcardially perfused with 0.1 M PBS, 0.015% digitonin followed by 4% paraformaldehyde in PBS.

Immunohistochemistry. Mice were deeply anesthetized with a mixture of ketamine (150 mg kg^{-1}) and xylazine (15 mg kg^{-1}), and transcardially perfused with 0.1 M PBS followed by 4% paraformaldehyde in PBS. Brains were removed and postfixed in 4% PFA for 24 h. Forty-micrometer free-floating coronal brain sections containing amygdala were collected using Leica vibratome. After blocking in 5% normal goat serum in 0.1 M PBS with 0.1% Triton X-100, brain sections were probed overnight with primary antibodies (chicken anti-eGFP (ab13970, 1:1,000; Abcam) for probing GFP in virally expressed GFP, rabbit anti-eGFP (G10362, 1:300; Thermo Fisher) for probing GFP in iPKR animals, rabbit anti-p-eIF2α S51 (3398, 1:300; Cell Signaling), chicken anti-mCherry (ab205402, 1:500; Abcam) and mouse anti-puromycin (MABE343, 1:1,000; Millipore)). After washing three times in 0.1 M PBS, brain sections were incubated with Alexa Fluor-conjugated secondary antibodies (1:200) in blocking buffer for 1.5 h at room temperature and mounted using Prolong Gold antifade mountant with 4,6-diamidino-2-phenylindole for nuclear counterstain. Imaging data were acquired using an SP8 confocal microscope (Leica) with 10× and 20× objective lenses with Leica LASX software and analyzed with ImageJ 2.0.0 using the Bio-Formats importer plug-in. To quantify the p-eIF2α S51 and puromycin signal intensity of each GFP-immunoreactive cell, we collected z stacks (10 optical sections with 0.563-µm step size) for three coronal sections per mouse ($n = 3$ mice) with 20× objective with 2× zoom. All compared samples were processed using the same protocol, and images were taken with equal microscope settings. Images were analyzed using ImageJ software. To compare across groups, we normalized all measures to the average intensity of the control group.

Statistics. No statistical methods were used to predetermine sample sizes, but our sample sizes are similar to those reported in previous publications[51,52]. No animals were excluded from the data analyses. Statistical analyses were performed using GraphPad Prism 8 (GraphPad Software). Data are expressed as mean ± standard error of the mean (s.e.m.). Data distribution was assumed to be normal, but this was not formally tested. Data from two groups were compared using two-tailed unpaired Student's *t*-test. Multiple group comparisons were conducted using one-way analysis of variance (ANOVA) or repeated-measures two-way ANOVA, with post hoc tests as described in the appropriate figure legend. Statistical analysis was performed with an α level of 0.05. The *P* values <0.05 were considered significant.

Reporting Summary. Further information on research design is available in the Nature Research Reporting Summary linked to this article.

Data availability

Sequence information for the targeting vector used to generate the iPKR knock-in mouse line is provided in Supplementary Data 1. Further data that support the findings of this study are available from the corresponding authors upon reasonable request.

References

51. Trinh, M. A. et al. The eIF2 α kinase PERK limits the expression of hippocampal metabotropic glutamate receptor-dependent long-term depression. *Learn. Mem.* **21**, 298–304 (2014).
52. Santini, E. et al. Exaggerated translation causes synaptic and behavioural aberrations associated with autism. *Nature* **493**, 411–416 (2013).

Acknowledgements

We thank M. Marmacz for expert technical assistance, C. Rice (The Rockefeller University) for providing the plasmid for HCV polyprotein, M. Ryan (University of St

Andrews) for the 2A plasmid, A. Klinakis (Biomedical Research Foundation Academy of Athens), A. Domingos and J. Friedman (The Rockefeller University) for the plasmid containing the STOP sequence and the *Eef1a1* targeting plasmid, P. Vandenabeele (Ghent University) for the PKRk plasmid, R. Kaufman (Sanford Burnham Prebys Medical Discovery Institute) for the Eif2s1 (S51A); CAG $Pr^{fl.Eif2s1.fl.GFP}$ mouse line and J. Pelletier (McGill University) for the *Col1a1*$^{TRE\ GFP.shmir4E.389}$ mouse line. We thank the Allen Brain Institute for providing AAV.*CAG Pr.DIO.tTA*. We thank all members of the Klann laboratory for critical feedback and discussions. This study was supported by National Institute of Health Grants (nos. NS034007 and NS047384) to E.K., a Howard Hughes Medical Investigator grant to N.H. and a Brain and Behavior Research Foundation NARSAD Young Investigator grant to P.S.

Author contributions

P.S., P.A. and N.H. conceptualized the iPKR system. P.S. and E.K. created the conceptual design of all in vivo work. P.A. designed and characterized the iPKR system in vitro and generated the iPKR mouse model under the supervision of N.H. P.S. carried out behavior training, and collected and analyzed in vivo and ex vivo data. P.H.-V. carried out behavior training. F.L. carried out and analyzed slice electrophysiology. A.G. helped with mouse behavior training. J.E.L. provided critical advice on behavioral design. P.S. and E.K. wrote the paper. All authors read and commented on the paper.

Competing interests

The authors declare no competing interests.

Additional information

Extended data is available for this paper at https://doi.org/10.1038/s41593-019-0568-z.

Supplementary information is available for this paper at https://doi.org/10.1038/s41593-019-0568-z.

Correspondence and requests for materials should be addressed to N.H. or E.K.

Reprints and permissions information is available at www.nature.com/reprints.

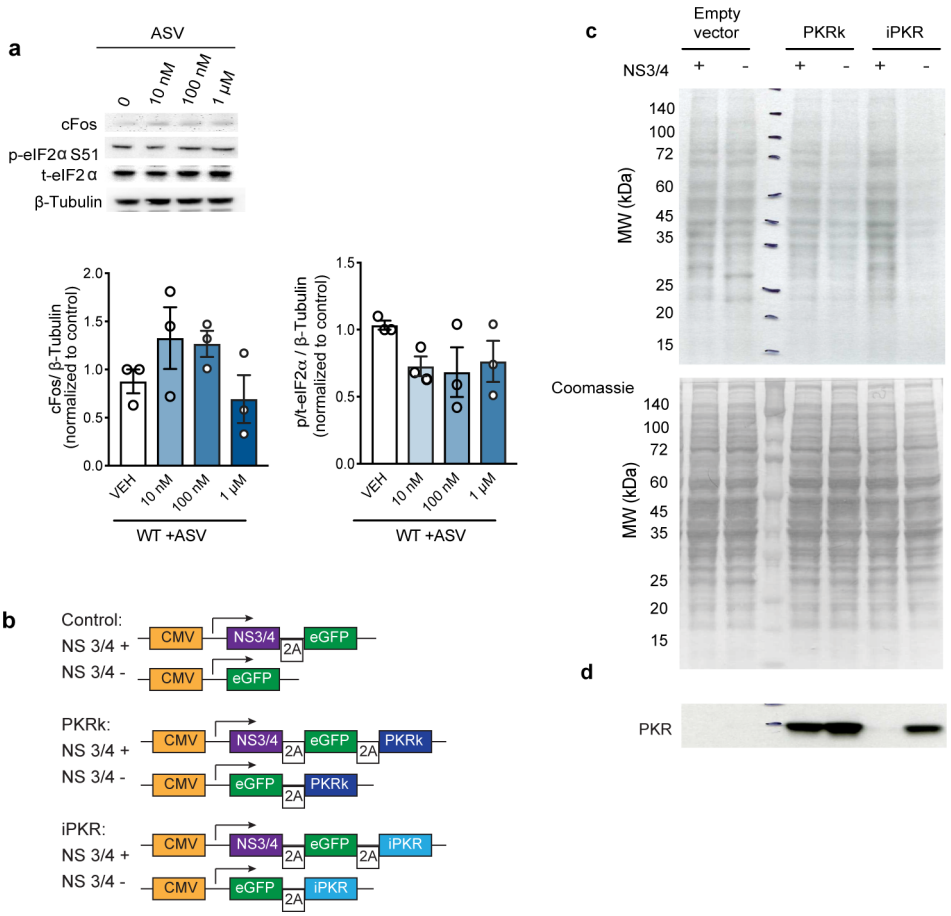

Extended Data Fig. 1 | Characterization of iPKR system. a) The toxicity of NS3/4 inhibitor ASV was determined by central i.c.v. administration of varying doses of the drug. Representative Western blots (top) shows the levels of cFos, phospho-eIF2α, total eIF2α, and control β-Actin band in response to the administration of ASV at the doses : 0, 10 nM, 100 nM (1 μM in 2 μl saline). Bar graph with individual data points shows quantification of cFOS (left) and phospho/total eIF2α (right) normalized to β-Actin. n=3 independent Western blots, 3 mice per group. One-way ANOVA. **b**) Schematic of the engineering approach for chemogenetic protein synthesis inhibitor plasmid construct consisting of NS3/4 protease, EGFP and iPKR kinase domain separated by 2A ribosome skipping sites under CMV promoter. Control plasmids harbored iPKR without NS3/4 protease or unmodified PKR kinase domain (PKRk). **c**) Metabolic S^{35} labeling of *de novo* translation *in vitro* showed significantly decreased translation in the presence of PKRk and iPKR (**p<0.01) but the translation block was lifted by the co-expression of NS3/4 protease that degrades iPKR (**p<0.01). n = 2 biological replicate lysates per group; One way ANOVA followed by Bonferroni's post-hoc test. F(5,6) = 19.01, **p=0.0013. **d**) iPKR expression is correspondingly regulated by NS3/4 protease (**p<0.01), whereas unmodified PKRk levels were unaltered by NS3/4 protease. n = 2 per group; One way ANOVA followed by Bonferroni's post-hoc test. F(5,6) = 22.21, ***p=0.0008. Data are presented as ± SEM.

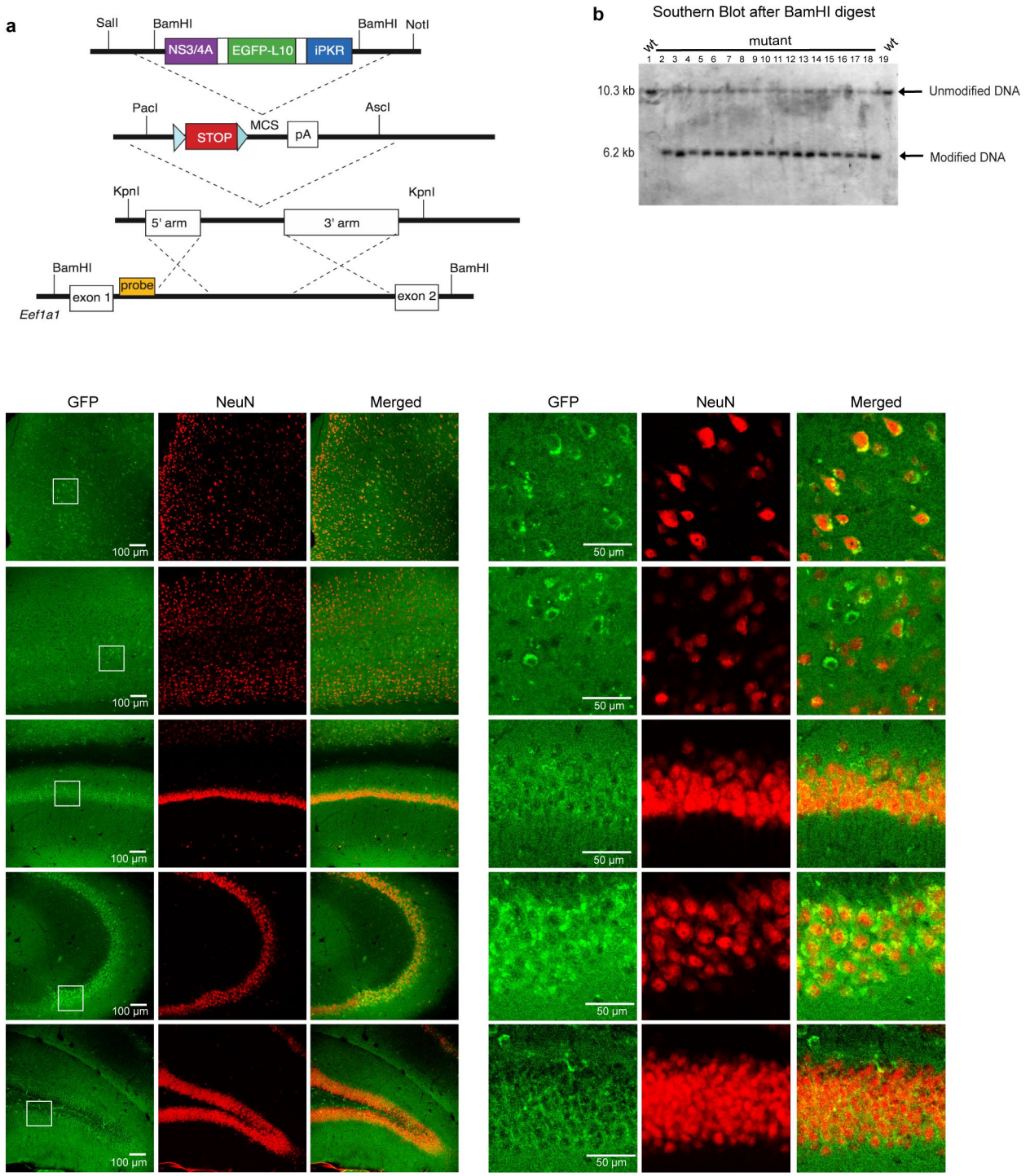

Extended Data Fig. 2 | Generation of iPKR mouse. a) Schematic showing the subcloning and targeting strategy of the multicistronic cassette containing loxP-flanked STOP cassette, NS3/4 protease, EGFP-L10, and iPKR kinase domain, which were separated by 2A ribosome skipping sites. The entire cassette was inserted between exon1 and exon 2 of *Eef1a1* genomic locus in mouse ES cells. Recognition site for the Southern blot probe is indicated. b) Southern blot after BamHI restriction enzyme-digested DNA isolated from embryonic stem cells using the probe indicated in a). Modified (6.2 kB kb) and unmodified (10.3 kB) DNA bands are indicated with arrows. In Nes iPKR brains, EGFP-L10 is expressed in the soma of neurons in the anterior cingulate cortex (c), somatosensory cortex (d), CA1 (e), CA3 (f) and dentate gyrus (g) consistent with NeuN expression. Insets show the corresponding brain areas at higher magnification.

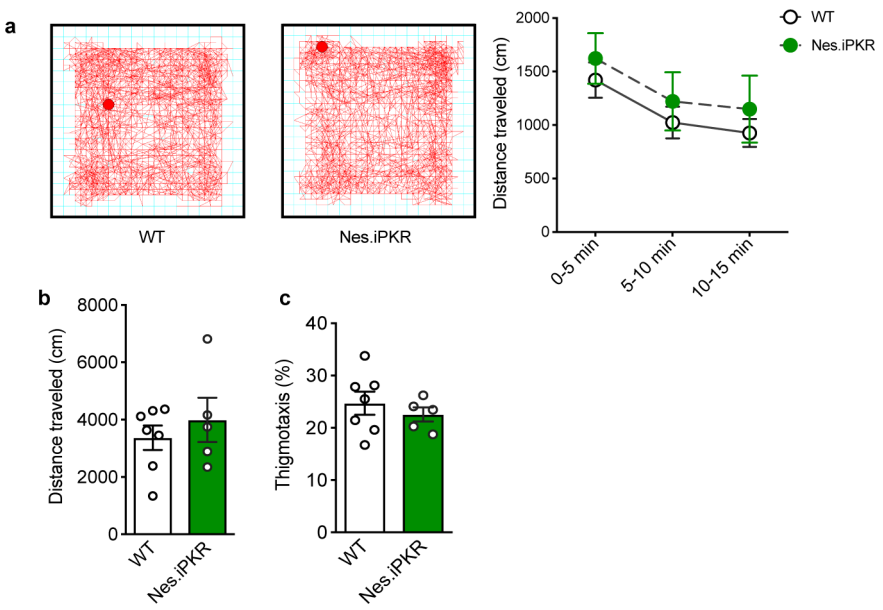

Extended Data Fig. 3 | Nes.iPKR mice display normal locomotor and anxiety related behavior. a) Nes.iPKR mice acclimated to the novel environment equivalent to the wildtype and exhibited c) normal locomotor activity in the open field test. d) Nes.iPKR animals displayed normal thigmotaxis as assessed by % distance traveled in the center compared to total distance. n = 5–7 per group; RM One-way ANOVA for (a) and Unpaired t-test for (c) and (d).

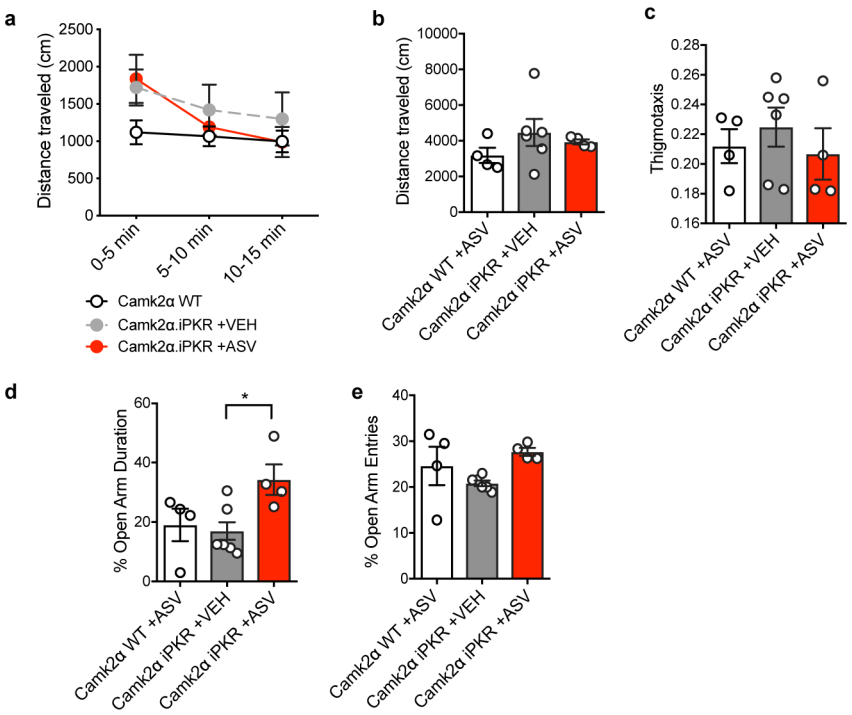

Extended Data Fig. 4 | General translation inhibition in CamK2α principal neurons. Blocking protein synthesis in CamK2α principal neurons in LA did not affect acclimation to a novel environment (**a**), total locomotor activity (**b**) or thigmotaxis, assessed by % distance traveled in center compared to total distance (**c**). **d**) In the elevated plus maze, however, animals with protein synthesis blocked in CamK2α principal neurons exhibited reduced anxiety i.e. increased %open arm duration (*$p<0.05$) compared to vehicle treated CamK2α iPKR mice and CamK2α wildtype mice even though they make equivalent entries to the open arm (**e**). n = 4-5 per group. RM Two-way ANOVA for a), One-way ANOVA followed by Bonferroni's post-hoc test for (b), (c), (d) and (e).

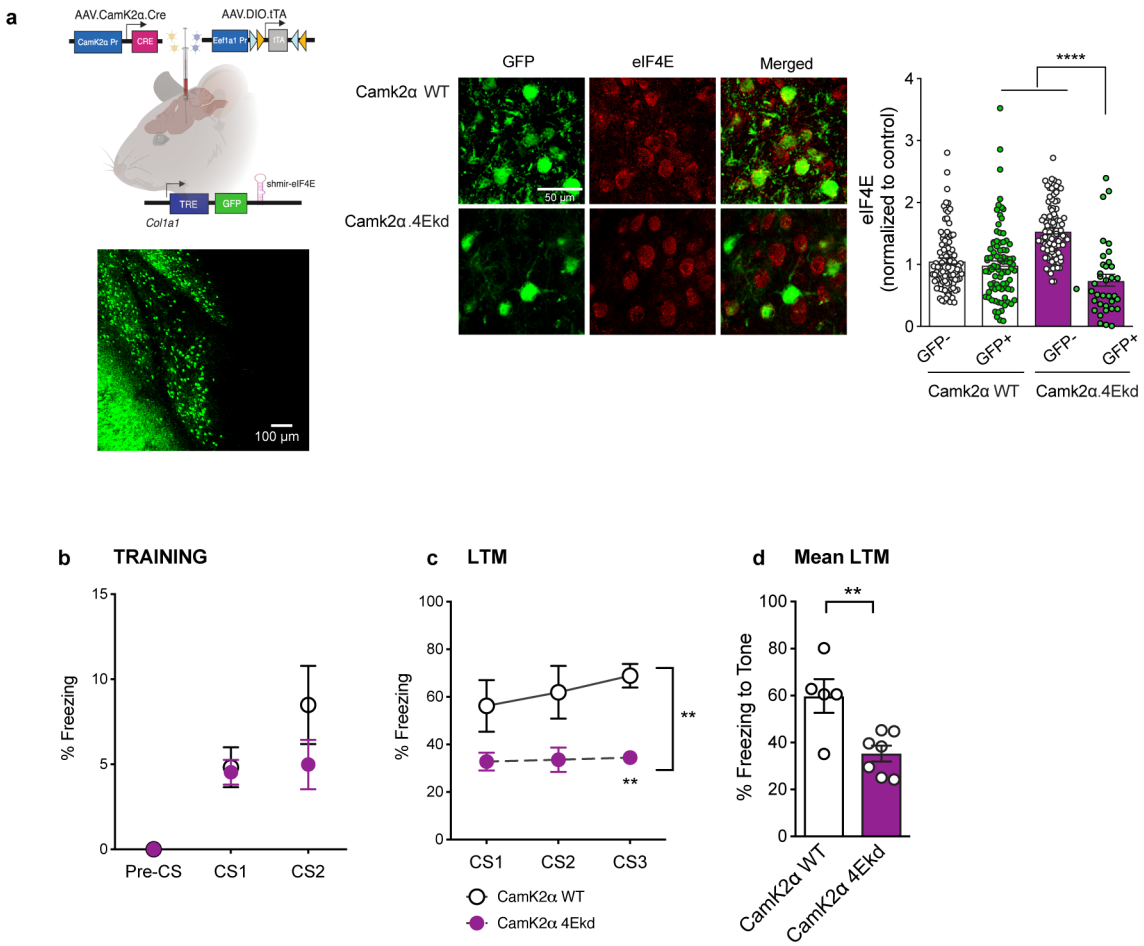

Extended Data Fig. 5 | Blocking cap-dependent translation in LA CamK2α principal neurons. a) Alternate strategy of blocking translation in CamK2α principal neurons in LA using cre-tet regulated synthetic micro-RNA targeted against eIF4E. Col1a1.TRE.GFP.shmir4E mice were bilaterally injected in the lateral amygdala with AAV1.CamK2α.Cre and AAV9.DIO.tTA, and placed off dox diet for 10 days before training. **b**) eIF4E protein level was significantly decreased in GFP+ neurons that express shmir4E. Two-way ANOVA with Bonferroni's post-hoc test. Genotype X GFP interaction: $F(1,311) = 32.29$, ****$p<0.0001$; GFP: $F(1,311) = 45.32$, ****$p<0.0001$. **c**) CamK2α 4Ekd mice learned the association between CS and US during training. RM Two-way ANOVA with Bonferroni's post-hoc test. CS: $F(2,14) = 17.54$, ***$p=0.0002$. **d**) Cued LTM was severely impaired across all three CS presentations. n=8 per group; RM Two-way ANOVA with Bonferroni's post-hoc test. $F(10,20) = 15.65$, **$p=0.0027$. d) Mean cTC LTM was significantly impaired in CamK2α 4Ekd mice compared to wildtype (***$p<0.001$). n = 8 per group; Unpaired t-test. Data are presented as ± SEM.

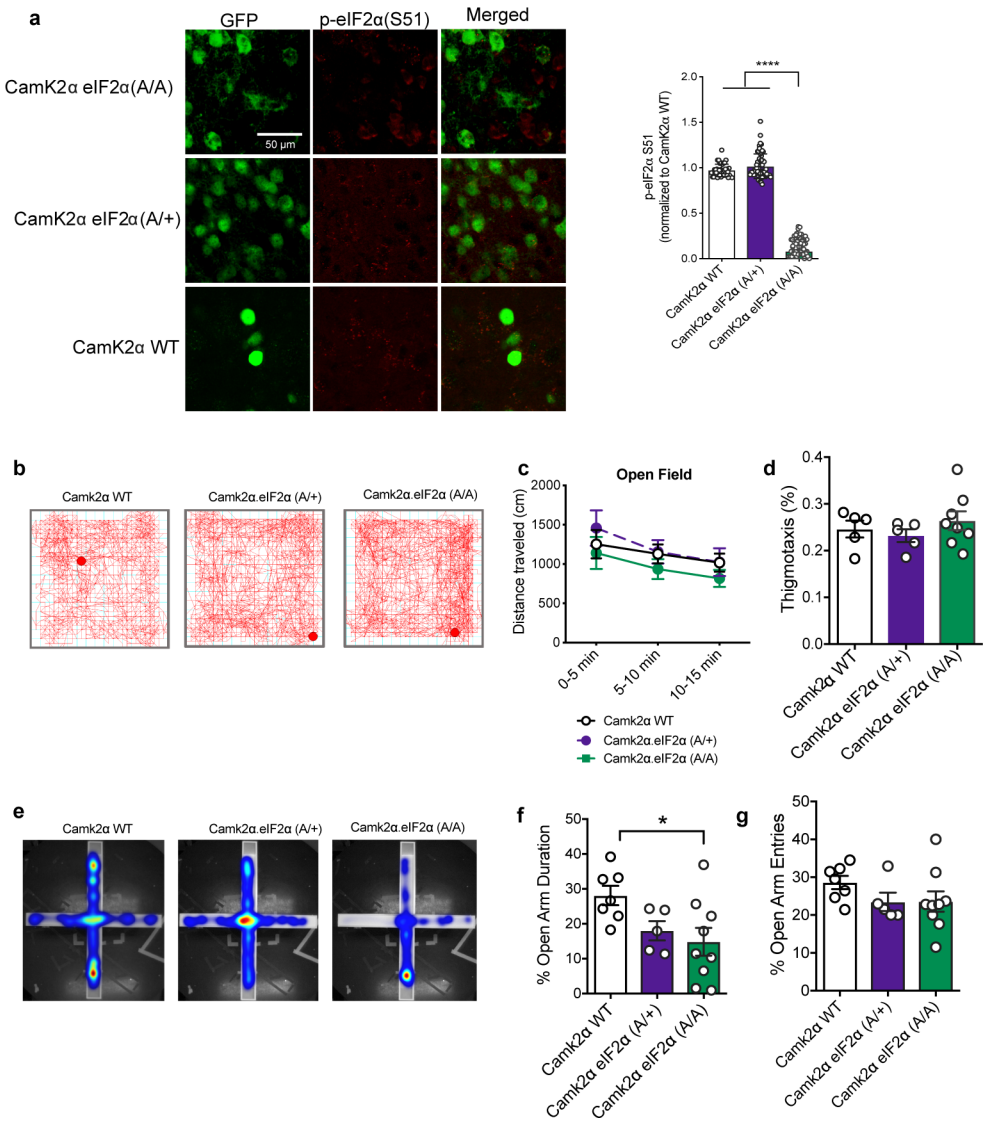

Extended Data Fig. 6 | Characterization of mice expressing phosphomutant eIF2α in LA CamK2α principal neurons. a) eIF2α phosphorylation at S51 was significantly reduced in GFP+ neurons in CamK2α.eIF2α (A/A) mice compared to GFP- neurons, as well as GFP+ neurons in CamK2α.WT mice (****p<0.001). (n = 60–74 per group, 3 animals); One-way ANOVA with Bonferroni's post-hoc test. F (2, 154) = 1055, ****p<0.0001. **b**) Representative motion traces from the open field test for CamK2α.WT, CamK2α.eIF2α(A/+) and CamK2α eIF2α (A/A) mice. **c**) In the open field test, CamK2α.eIF2α (A/A) mice acclimated to the novel environment and had comparable spontaneous locomotion compared to the CamK2α.WT mice and CamK2α. eIF2α (A/+) mice. RM One-way ANOVA. **d**) Bar graphs representing thigmotaxis, i.e. %time spent in center compared to total distance traversed in the open field arena for the three groups. One-way ANOVA. **f**) In the elevated plus maze, CamK2α.eIF2α (A/A) mice spent a significantly higher duration in the open arm compared to CamK2α WT mice (**g**) (*p<0.05) indicating anxiety like behavior, even though they made equivalent entries to the open arm. One-way ANOVA with Bonferroni's post-hoc test. F(2,17) = 3.775, *p=0.0440. Data are presented as +/- SEM.

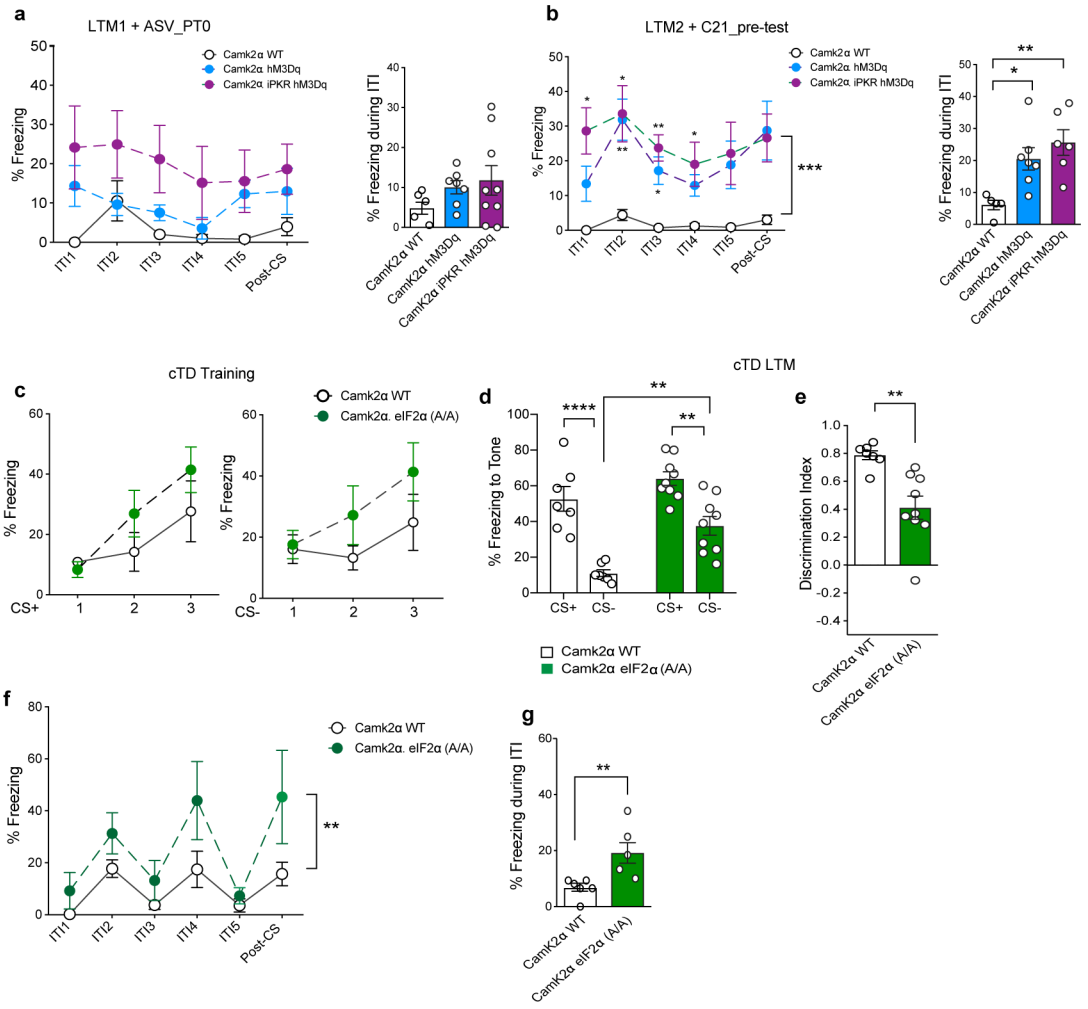

Extended Data Fig. 7 | Artificial chemogenetic activation of LA CamK2α principal neurons. a) All groups of mice - CamK2α. iPKR hM3Dq, CamK2α. hM3Dq and CamK2α WT, exhibited low freezing during ITI in LTM1. XY plots showing %freezing during individual ITIs and Post-CS (left; RM Two-way ANOVA) and bar graphs showing mean %freezing during ITI (right; One-way ANOVA). n = 6–9 per group. **b**) During LTM2, administration of DREADD agonist C21 caused an increase in freezing during ITI for both CamK2α.hM3Dq and CamK2α. iPKR hM3Dq groups compared to CamK2α WT mice. XY plots showing %freezing during individual ITIs and Post-CS (left). n = 5–7 per group. RM Two-way ANOVA genotype: F(2,15)=12.63, ***p=0.0006). Bar graphs showing mean %freezing during ITI (right). One-way ANOVA with Bonferroni's post-hoc test. *p<0.05 and **p<0.01. **c**) CamK2α. eIF2α (A/A) mice displayed comparable learning in the diferential threat conditioning training for both CS+ (right) and CS- (left). **d**) However, in the LTM test, they displayed significant increase in CS- response compared to CamK2α WT mice (**p<0.01). Two-way ANOVA with Bonferroni's post-hoc test. CS: F(1,28) = 49.18, ****p<0.0001; Genotype: F(1,28) = 15.26, ***p=0.0005. **e**) The cTD discrimination index was significantly lower for CamK2α. eIF2α (A/A) mice (**p<0.01) relative to controls. n=7-10 per group; Unpaired t-test. **f**) Besides stimulus generalization, CamK2α. eIF2α (A/A) mice also displayed cognitive inflexibility and could not stop freezing after the tone offset, and thus had significantly higher freezing rate during the ITIs. RM Two-way ANOVA with Bonferroni's post-hoc test. Genotype: F(1,10) = 16.70, **p=0.0022. **g**) Mean freezing response during ITI is significantly increased in CamK2α. eIF2α (A/A) mice (**p=0.0097) . n=7-10 per group; Unpaired t-test. Data are presented as mean +/- SEM.

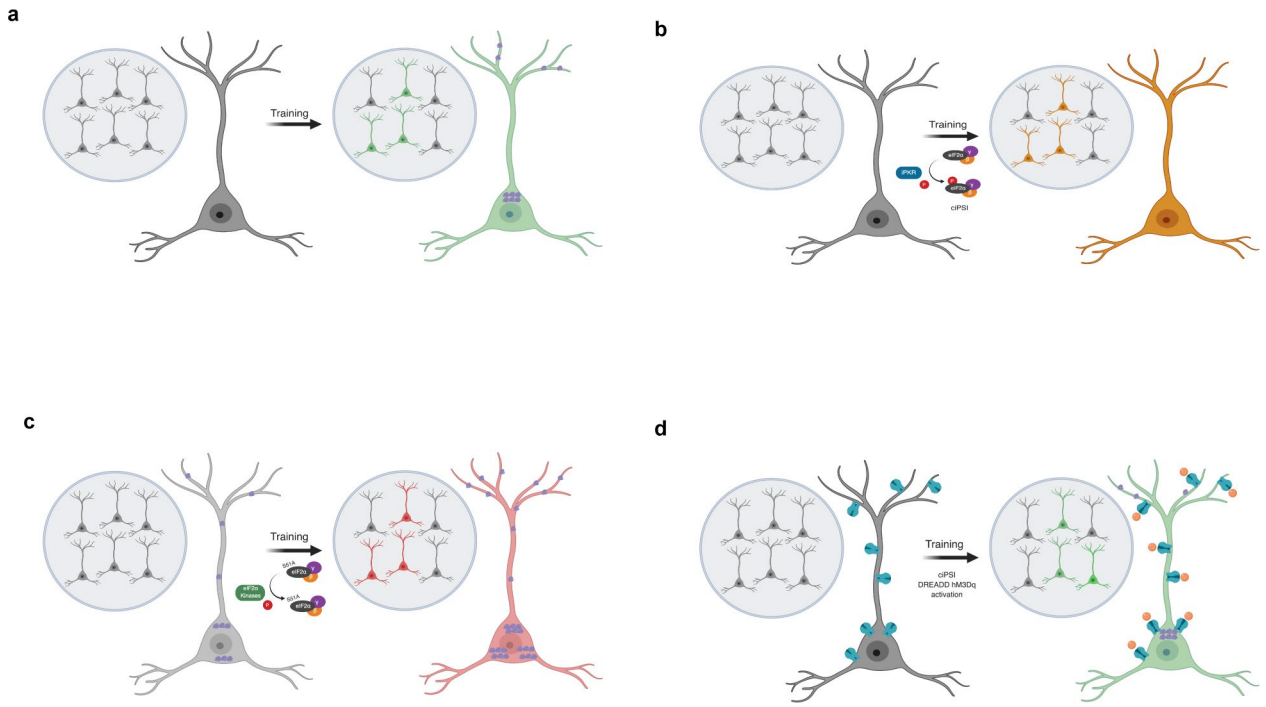

Extended Data Fig. 8 | Model for protein synthesis regulation during long-term memory consolidation. a) In wild-type mice, threat conditioning leads to a spatiotemporally regulated increase in somatic and dendritic protein synthesis that stabilizes the memory trace. **b**) Application of ciPSI system prevents the coordinated increase in cell-wide translation leading to impaired LTM. **c**) Dephosphorylation of eIF2α enhances general translation, but it is dysregulated and unable to coordinate the cell-wide translation program to store a complex memory trace, resulting in memory generalization. **d**) Artificial reactivation of the amygdala principal neurons after protein synthesis inhibition-mediated amnesia leads to an increase in translation but does not restore synapse specificity and thus leads to memory generalization.

nature research

Corresponding author(s): Eric Klann, Nathaniel Heintz

Last updated by author(s): 11/14/2019

Reporting Summary

Nature Research wishes to improve the reproducibility of the work that we publish. This form provides structure for consistency and transparency in reporting. For further information on Nature Research policies, see Authors & Referees and the Editorial Policy Checklist.

Statistics

For all statistical analyses, confirm that the following items are present in the figure legend, table legend, main text, or Methods section.

n/a	Confirmed	
☐	☒	The exact sample size (*n*) for each experimental group/condition, given as a discrete number and unit of measurement
☐	☒	A statement on whether measurements were taken from distinct samples or whether the same sample was measured repeatedly
☐	☒	The statistical test(s) used AND whether they are one- or two-sided *Only common tests should be described solely by name; describe more complex techniques in the Methods section.*
☐	☒	A description of all covariates tested
☐	☒	A description of any assumptions or corrections, such as tests of normality and adjustment for multiple comparisons
☐	☒	A full description of the statistical parameters including central tendency (e.g. means) or other basic estimates (e.g. regression coefficient) AND variation (e.g. standard deviation) or associated estimates of uncertainty (e.g. confidence intervals)
☐	☒	For null hypothesis testing, the test statistic (e.g. *F*, *t*, *r*) with confidence intervals, effect sizes, degrees of freedom and *P* value noted *Give P values as exact values whenever suitable.*
☒	☐	For Bayesian analysis, information on the choice of priors and Markov chain Monte Carlo settings
☒	☐	For hierarchical and complex designs, identification of the appropriate level for tests and full reporting of outcomes
☒	☐	Estimates of effect sizes (e.g. Cohen's *d*, Pearson's *r*), indicating how they were calculated

Our web collection on statistics for biologists contains articles on many of the points above.

Software and code

Policy information about availability of computer code

Data collection	FreezeFrame 4, Activity Monitor 6.02, Ethovision XT13, Leica LASX, Protein Simple - Alpha Imager 3.4
Data analysis	We used GraphPad Prism 8 to analyze behavior data. We used ImageJ 2.0.0-rc-69/1.52p to analyze confocal images and Western Immunoblots.

For manuscripts utilizing custom algorithms or software that are central to the research but not yet described in published literature, software must be made available to editors/reviewers. We strongly encourage code deposition in a community repository (e.g. GitHub). See the Nature Research guidelines for submitting code & software for further information.

Data

Policy information about availability of data

All manuscripts must include a data availability statement. This statement should provide the following information, where applicable:

- Accession codes, unique identifiers, or web links for publicly available datasets
- A list of figures that have associated raw data
- A description of any restrictions on data availability

All data generated or analyzed during this study are included in this article and supplementary files.

Field-specific reporting

Please select the one below that is the best fit for your research. If you are not sure, read the appropriate sections before making your selection.

☒ Life sciences ☐ Behavioural & social sciences ☐ Ecological, evolutionary & environmental sciences

For a reference copy of the document with all sections, see nature.com/documents/nr-reporting-summary-flat.pdf

Life sciences study design

All studies must disclose on these points even when the disclosure is negative.

Sample size	Sample size were estimated based on existing published research.
Data exclusions	None
Replication	Each experiment represents several independent cohorts, as described in the methods.
Randomization	Mice were randomly allocated to experimental groups.
Blinding	Data was analyzed by researchers blind to genotypes/ experimental manipulations.

Reporting for specific materials, systems and methods

We require information from authors about some types of materials, experimental systems and methods used in many studies. Here, indicate whether each material, system or method listed is relevant to your study. If you are not sure if a list item applies to your research, read the appropriate section before selecting a response.

Materials & experimental systems

n/a	Involved in the study
☐	☒ Antibodies
☐	☒ Eukaryotic cell lines
☒	☐ Palaeontology
☐	☒ Animals and other organisms
☒	☐ Human research participants
☒	☐ Clinical data

Methods

n/a	Involved in the study
☒	☐ ChIP-seq
☒	☐ Flow cytometry
☒	☐ MRI-based neuroimaging

Antibodies

Antibodies used

Biotin (abcam ab53494, 1:500), p-eIF2alpha (Cell Signaling 9721, 1:300), p-eIF2alpha Ser51 (Cell Signaling 3398, 1:300), t-eIF2alpha (Cell Signaling 9722, 1:500), PKR (Cell Signaling 3072, 1:300), ATF4 (Santa Cruz sc-200, 1:300), p-ERK1/2 Thr202/Tyr204 (Cell Signaling 9101, 1:1000), ERK1/2 (Cell Signaling 9102, 1:1000), p-S6 (Ser240/244) (Cell Signaling 5364, 1:500), t-S6 (Cell Signaling 2317, 1:500), Puromycin (Millipore MABE343, 1:1000), beta-Tubulin (Sigma-Aldrich T8328, 1:5000), beta-Actin (Sigma-Aldrich A5316, 1:5000), cFos (Santa Cruz sc-253, 1:300), GFP (Abcam ab13970, Thermo Fisher G10362, 1:300), mCherry (Abcam ab205402, 1:500), Gadd34 (Proteintech #10449-1-AP, 1:1000)

Validation

Biotin: synthetic peptide against KLH (biotin), website states specific to free biotin and biotinylated antibody and proteins. Primary literature citing use of this antibody: Stypulkowski, E et al. Sci Signal 2018. PMID: 29295957

p-eIF2alpha Ser51: synthetic phosphopeptide corresponding to residues surrounding Ser51 of eIF2alpha. website states the antibody detects endogenous eIF2alpha only when phosphorylated at Ser51 and does not recognize eIF2alpha phosphorylated at other sites. Primary literature citing use of this antibody: Jiang et al. Nat Comm .2016. PMID: 27416896

t-eIF2alpha: synthetic peptide against carboxy terminal sequence of eIF2alpha. websites states the antibody is specific to total eIF2alpha protein; Primary literature citing use of this antibody:Jiang et al. Nat Comm .2016. PMID: 27416896

PKR: synthetic peptide against PKR carboxy terminal (aa 500-600). website states antibody was knockout validated and does not cross-react with other eIF2alpha kinases. Primary literature citing use of this antibody: Ikegami et al. PLoS Pathogens 2009. PMID:19197350

ATF4: synthetic peptide against C terminus of CREB-2 (ATF4). website states antibody was knockout validated and is specific to ATF4 protein. Primary literature citing use of this antibody: Lin et al. Mol Neurobiol 2015. PMID: 24915969

p-ERK1/2 Thr202/Tyr204: synthetic phosphopeptide corresponding to residues surrounding Thr202/Tyr204 of p44 ERK1 protein. website states antibody is specific for endogenous levels of p44 and p42 MAP Kinase (ERK1 and ERK2) when phosphorylated either individually or dually at Thr202 and Tyr204 of ERK1 (Thr185 and Tyr187 of ERK2), and does not cross-react with the non-phosphorylated ERK1/2. Primary literature citing use of this antibody: Beirowski et al. PNAS 2017. PMID: 28484008

t-ERK1/2: synthetic peptide derived from a sequence in the C-terminus of rat p44 MAP kinase. website states antibody is siRNA validated and is specific for total p44/42 MAP kinase (ERK1/2) protein. Primary literature citing use of this antibody: Beirowski et al. PNAS 2017. PMID: 28484008

p-S6 (Ser240/244): monoclonal antibody generated using a synthetic phosphopeptide corresponding to residues surrounding Ser240 and Ser244 of human ribosomal protein S6. Primary literature citing use of this antibody: Beirowski et al. PNAS 2017. PMID: 28484008

t-S6: mouse monoclonal antibody generated using a recombinant fusion protein corresponding to full-length human S6 ribosomal protein. Primary literature citing use of this antibody: Beirowski et al. PNAS 2017. PMID: 28484008

Puromycin: monoclonal antibody generated using synthetic peptide against puromycin from Streptomyces alboniger. website states antibody detects puromycin-incorporated neosynthesized proteins treated with puromycin only and has been evaluated by western blotting in HEK293 cell lysates treated with puromycin. Primary literature citing use of this antibody:Primary literature citing use of this antibody: Beirowski et al. PNAS 2017. PMID: 28484008

beta-Tubulin: monoclonal antibody derived from the hybridoma AA2 produced by fusion of mouse myeloma cells and splenocytes from BALB/c mice immunized with purfied bovine tubulin. website states antibody reacts with beta-tubulin, types I, II, III and IV. Primary literature citing use of this antibody: Santini et al. Science Signal 2017. PMID: 29114037

beta-actin: monoclonal antibody derived from hybridoma AC-74 produced by fusion of mouse myeloma cells and splenocytes from mice immunized with synthetic beta-cytoplasmic actin N-terminal peptide, conjugated to biotin (KLH). website states antibody is specific for beta-actin. Primary literature citing use of this antibody: Yu et a. Nat Comm 2015. PMID: 25998442

cFos: polyclonal antibody generated using epitope mapped within an internal region of c-Fos of human origin. Primary literature citing use of this antibody: Yu, H et al. J Neuroscience 29(13): 4056-64. PMID:19339601

Chicken anti-GFP: synthetic full length protein corresponding to GFP. website states antibody was validated using western blot and transgenic animals. Primary literature citing use of this antibody: Doyle et al. Cell 2008. PMID: 19013282; Rabbit anti-GFP: Monoclonal antibody generated using full length GFP. Viswanathan S et al. Nat Methods 2015. PMID: 25915120

mCherry: synthetic full length protein corresponding to mCherry. website states antibody was validated using western blot and transgenic mice. Primary literature citing use of this antibody: Moreno et al. Curr Biol 2019. PMID: 30554899

Gadd34: Knock-out validated polyclonal antibody, generated in rabbits using GADD34 fusion protein Ag0578. Primary literature citing use of this antibody: Dalton et al. Br J Cancer 2013. PMID: 23412101

Eukaryotic cell lines

Policy information about cell lines

Cell line source(s)	293T cells from ATCC, 129S6/SvEvTac embryonic stem cells
Authentication	293T cells from ATCC: website states that routine cell line authentication is carried out with short tandem repeat profiling, cellular morphology, karyotyping and cytochrome C oxidase I assay testing. 129S6/SvEvTac embryonic stem cells: These cells were generated, and routinely authenticated with karyotyping and imumnostaining for pluripotency markers by the Rockefeller University Gene targeting center.
Mycoplasma contamination	Cell lines were not contaminated with mycoplasma.
Commonly misidentified lines (See ICLAC register)	None

Animals and other organisms

Policy information about studies involving animals; ARRIVE guidelines recommended for reporting animal research

Laboratory animals	Mus musculus, iPKR mice 5x backcrossed to C57Bl6J, male and female, 10-15 weeks old
Wild animals	None
Field-collected samples	None
Ethics oversight	University Animal Welfare Committee and Institutional Biosafety Committee approved and provided guidance on the study protocol.

Note that full information on the approval of the study protocol must also be provided in the manuscript.